Regular Article

Vibration and damping analyses of sandwich cylindrical and conical shells using meshfree method

Zhen Li[1], Qingshan Wang[1,a], Rui Zhong[1], Bin Qin[2,3,4], Wen Shao[1]

[1] State Key Laboratory of High Performance Complex Manufacturing, Central South University, Changsha 410083, People's Republic of China
[2] Key Laboratory of Traffic Safety on Track, Ministry of Education, School of Traffic and Transportation Engineering, Central South University, Changsha 410075, People's Republic of China
[3] Joint International Research Laboratory of Key Technology for Rail Traffic Safety, Central South University, Changsha 410075, People's Republic of China
[4] National and Local Joint Engineering Research Center of Safety Technology for Rail Vehicle, Central South University, Changsha 410075, People's Republic of China

Abstract The vibration and damping characteristics of sandwich shells including cylindrical and conical shells with viscoelastic core layer are investigated by using a meshfree method. The energy principle and Donnel shell hypothesis are applied to establish the theoretical formulations of sandwich shells. The displacement components of the viscoelastic core are expressed as those of base and constraining layers by using continuity condition. The displacement variables of sandwich shells expanded by the meshfree shape function and axial and circumferential directions Fourier series. The validation including accuracy and reliability of the presented method is verified by comparing the presented results with the corresponding results of the existing literatures. Furthermore, the vibration and damping behaviors of sandwich shells are analyzed by investigating the effects of geometric dimensions, material properties and boundary conditions on the natural frequencies and modal loss factors of sandwich shells, which contributes to the preliminary design of sandwich shells with viscoelastic core layer.

1 Introduction

As the typical representative of novelty intelligent multifunctional structure, sandwich shell structure is made up of three important components including base layer (lower panel), viscoelastic core layer (core structure) and constraining layer (upper panel). Comparing with the traditional shell engineering structure, sandwich shell structure has excellent capacity in energy dissipation and absorption, high temperature and pressure resistances, low-weight and high structural efficiency. Based on the above excellent structural properties, sandwich shell structure has been promoted to various engineering applications including underwater submarine, launch vehicle, spacecraft and pressure vessels and so on. However, the vibration and damping performances with regard to sandwich shells have important influences in the reliability and stability of engineering structure composed of sandwich shell structure. Thus, the investigations of vibration and damping characteristic have great significance to the structural designation and safety performance evaluation of sandwich shell structure.

Yadav et al. [1] analyzed the forced vibration behaviors of sandwich shell contain cellular core and thin panels based on high-order shear deformation theory (HSDT) by employing Galerkin, incremental harmonic balance and arclength continuation methods. Yang et al. [2] proposed a three-dimensional numerical model of sandwich shallow shells under various boundary conditions for investigating its vibration characteristics by using Rayleigh–Ritz and modified three-dimensional Fourier series approaches. Li et al. [3] studied the vibration and thermal buckling behaviors of sandwich shells made up of face panels with functionally graded material (FGM) and tunable auxetic honeycomb core by employing complex modulus approach and Hamilton's principle. Wang et al. [4] studied the vibration behaviors of sandwich cylindrical shell with composite pyramidal truss core by employing theoretically in conjunction with experimentally. Wang et al. [5, 6] put forward a semi-analytical approach for investigating the vibration behaviors of sandwich shell and panel with FGM under various boundary conditions by using modified Fourier series method based on first-order shear deformation theory (FSDT). Taati et al. [7, 8] focused on the vibration behaviors with regard to sandwich cylindrical shell which consists of carbon nanotube-reinforced face sheets and metal foam core under fluid flow by establishing fluid–structure coupling model based on classical shell theories. Yang et al. [9] discussed the vibration and damping characteristics of sandwich shells with pyramidal truss-like cores by applying finite element and Rayleigh–Ritz methods. Karimiasl et al. [10] investigated the nonlinear vibration behaviors of sandwich shell composed of magnetorheological layer flexible core layer and composite layer

based on the Hamilton's principle and Reddy's third-order shear deformation theory. Li et al. [11] studied the free flexural vibration behaviors of sandwich shell with porous honeycomb core based on Flügge's shell theory and Gibson's formula in conjunction with experiments. Fu et al. [12] investigated the vibration behaviors of sandwich shells composed of functionally graded material skins and isotropic core subjected to elastic foundations by applying generalized differential quadrature approach. Sobhani et al. [13] researched the vibration characteristics of sandwich coupled shells under boundary conditions based on FSDT and Donnell's shell theory. Kumar et al. [14] established two-dimensional finite element model for studying the vibration behaviors of sandwich shell by using first and higher order zigzag theories. Singha et al. [15] analyzed the vibration behaviors of sandwich conical shell made up of composite panels and synthetic foam core. Li et al. [16, 17] proposed an analytical model of shells that consist of hexagon honeycomb core and fiber-reinforced composite skins by employing Hamilton's principle and Galerkin approach.

Sobhani et al. [18, 19] analyzed the circumferential vibration of sandwich coupled shell structures subjected to various elastic boundary conditions by using generalized differential quadrature strategy and Hamilton's method. Xue et al. [20] investigated the damping and vibration performances of sandwich cylindrical shell with gradient core by means of experiments. Sofiyev et al. [21] discussed the vibration and bulking behaviors of sandwich cylindrical shell with different type coatings by applying FSDT. Chen et al. [22–25] presented a dynamics model to investigate the sandwich doubly-curved shallow shells subjected to simply supported boundary conditions by employing Navier method in conjunction with FSDT. Sayyad et al. [26–28] analyzed the vibration and bending behaviors of sandwich spherical and conical shells based on classical and high-order shear shell theories and Hamilton's principle. F. Bahranifard et al. [29–31] investigated the dynamic characteristics of sandwich-truncated conical shells made up of face sheets and porous core by using Chebyshev–Ritz method. Li et al. [32] presented a novelty theoretical analysis model of sandwich cylindrical shell with composite pyramidal truss and damp coating subjected to elastically supported boundary conditions by applying Rayleigh–Ritz approach. Zheng et al. [33] provided an accurate numerical model of sandwich shell made up of composite panel layer and magnetorheological core by means of wave propagation technique, Hamilton's principle and linear viscoelastic scheme. Biswal et al. [34, 35] discussed the vibration and damping behaviors of sandwich shells with three layers including base layer, viscoelastic core and constraining layer based on Hamilton's principle by employing finite element method. Soureshjani et al. [36] proposed a semi-analytical approach for investigating the vibration characteristics with regard to coupled sandwich conical shell structures under various boundary conditions. Parand et al. [37, 38] analyzed the vibration behaviors of sandwich shell with viscoelastic interface and FGM core by employing Fourier series in conjunction with differential quadrature method. Sahu et al. [39] researched the vibration and damping behaviors of sandwich shell panels including viscoelastic core layer and functional graded layer based on FSDT by utilizing finite element method.

This paper proposes an unified numerical method for investigating the vibration and damping behaviors of sandwich shell structure including conical shell and cylindrical shell by employing the meshfree method. The sandwich shell structures are composed of based layer, viscoelastic layer and constraining layer, and the theoretical formulations of sandwich shells are derived based on energy principle and Donnel shell assumption in conjunction with FSDT. Only flexural and axial deformations are allowed in the base layer and constraining layer; only shear strains is allowed in the viscoelastic layer. Using the continuity condition in interface between the layers, the displacement components of the viscoelastic core are replaced by those of base and constraining layers. The displacement components of sandwich shell are approximated by employing Fourier series in conjunction with shape function produced by meshfree Tchebychev radial point interpolation method. The validation of the presented approach is verified by the comparison results of presented approach and existing literatures. Based on the above proposed method, the vibration and damping analyses of sandwich shells are performed by investigating the influences of the parameters including geometric dimension, boundary conditions and material properties on the vibration and modal loss factor of sandwich shell.

2 Theoretical modeling

2.1 Introduction of model

As shown in Fig. 1, sandwich conical shell structure with isotropic is made up of three layers including based layer, viscoelastic core layer and constraining layer. For convenience, the sandwich conical shell structure is described by employing orthogonal curvilinear coordinate systems, and the above coordinate systems are established at the middle surfaces of each layer. α and L denote semi-vertex and length with respect to sandwich conical shell structure of each layer; R_{i0} ($i = s, v, c$) represents the left side of sandwich conical shell structure of each layer and the subscript characters s, v and c of R_{i0} indicate base layer, viscoelastic core layer and constraining layer. Meanwhile, it is worth mentioning that the conical shell structure can be regard as cylindrical shell structure when the geometric characteristic parameter α is selected as 0.

2.2 Meshfree shape function

The meshfree shape function produced by Tchebychev radial point interpolation method is applied in the proposed approach. The above meshfree shape function can be regard as the combination of the radial basis function and Tchebychev polynomials, the corresponding expression is written as follow.

$$u(x) = \sum_{i=1}^{N} R_i(x)a_i + \sum_{j=1}^{N_t} \tau_j(x)b_j = \boldsymbol{R}^T(x)\boldsymbol{a} + \boldsymbol{T}^T(x)\boldsymbol{b} \tag{1}$$

where the symbols of $R_i(\boldsymbol{x})$ and $\tau_j(\boldsymbol{x})$ represent radial and Tchebychev polynomial basis functions; N and N_t denote the numbers of the above corresponding basis functions. The concrete expression of Tchebychev polynomial basis function with one-dimensional can be expressed as follows:

$$\boldsymbol{T}(\boldsymbol{x}) = \begin{bmatrix} T_0(x) \ T_1(x) \ \cdots \ T_p(x) \ \cdots \end{bmatrix}^T \tag{2}$$

$$T_k(x) = \cos[k \cos^{-1}(x)] \quad , \quad k = 0, \ 1, \ 2 \cdots \tag{3}$$

The radial basis function of meshfree shape function is determined by selecting multi-quadrics (MQ) radial basis function; the specific expression of radial basis function is described as follows:

$$R_i(\boldsymbol{x}) = \begin{bmatrix} r_i^2 + (\alpha_c d_c)^2 \end{bmatrix}^q \tag{4}$$

where d_c denotes nodal mean spacing and r_i represents the distance between interested node and divided node. For determining the unknown variables a_i and b_j, the divided nodes need to be introduced into Eq. (1) for establishing a set of linear equation, the matrix expression of the above linear equation can be written as the following form:

$$\boldsymbol{U}_s = \boldsymbol{R}_0\boldsymbol{a} + \boldsymbol{T}_{N_t}\boldsymbol{b} \tag{5}$$

$$\boldsymbol{a} = \begin{bmatrix} a_1 \ a_2 \ \cdots \ a_N \end{bmatrix}^T, \quad \boldsymbol{b} = \begin{bmatrix} b_1 \ b_2 \ \cdots \ b_{N_t} \end{bmatrix}^T \tag{6}$$

where the concrete expressions of the matrices $\boldsymbol{U}s, \boldsymbol{R}_0, \boldsymbol{T}_{N_t}$ can be described as follows:

$$\boldsymbol{U}_s = \begin{bmatrix} u_1 \ u_2 \ \cdots \ u_N \end{bmatrix}^T \tag{7}$$

$$\boldsymbol{R}_0 = \begin{bmatrix} R_1(r_1) & R_2(r_1) & \cdots & R_N(r_1) \\ R_1(r_2) & R_2(r_2) & \cdots & R_N(r_2) \\ \vdots & \vdots & \ddots & \vdots \\ R_1(r_N) & R_2(r_N) & \cdots & R_N(r_N) \end{bmatrix} \tag{8}$$

$$\boldsymbol{T}_{N_t} = \begin{bmatrix} T_0(x_1) & T_1(x_1) & \cdots & T_{N_t}(x_1) \\ T_0(x_2) & T_1(x_2) & \cdots & T_{N_t}(x_2) \\ \vdots & \vdots & \ddots & \vdots \\ T_0(x_N) & T_1(x_N) & \cdots & T_{N_t}(x_N) \end{bmatrix}_{N \times N_t} \tag{9}$$

The definition expression of r_k in $R_i(r_k)$ of Eq. (8) is shown as follows:

$$r_k = x_k - x_i \tag{10}$$

In order to solving Eq. (5) advantageously, the following constraint equations need to be applied.

$$\sum_{i=1}^{N} T_j(\boldsymbol{x}_i)a_i = \boldsymbol{T}_{N_t}^T\boldsymbol{a} = 0 \quad , \quad j = 1, 2, \cdots, N_t \tag{11}$$

From Eqs. (5) and (11)

$$\overline{\boldsymbol{U}}_s = \begin{bmatrix} \boldsymbol{U}_s \\ \boldsymbol{0} \end{bmatrix} = \begin{bmatrix} \boldsymbol{R}_0 & \boldsymbol{T}_{N_t} \\ \boldsymbol{T}_{N_t}^T & \boldsymbol{0} \end{bmatrix} \begin{bmatrix} \boldsymbol{a} \\ \boldsymbol{b} \end{bmatrix} = \boldsymbol{G}\boldsymbol{a}_0 \tag{12}$$

According to variable substitution, Eq. (1) can be revised as follows:

$$u(x) = \boldsymbol{R}^T(x)\boldsymbol{a} + \boldsymbol{T}^T(x)\boldsymbol{b} = \begin{bmatrix} \boldsymbol{R}^T(x) \ \boldsymbol{T}^T(x) \end{bmatrix} \begin{bmatrix} \boldsymbol{a} \\ \boldsymbol{b} \end{bmatrix}$$

$$= \begin{bmatrix} \boldsymbol{R}^T(x) \ \boldsymbol{T}^T(x) \end{bmatrix} \boldsymbol{G}^{-1}\bar{\boldsymbol{U}}_s = \bar{\boldsymbol{\Phi}}^T(x)\bar{\boldsymbol{U}}_s \tag{13}$$

$$\bar{\boldsymbol{\Phi}}^T(x) = \left[\boldsymbol{R}^T(x) \ \boldsymbol{T}^T(x) \right] \boldsymbol{G}^{-1}$$
$$= \left[\phi_1(x) \ \phi_2(x) \cdots \phi_N(x) \ \phi_{N+1}(x) \cdots \phi_{N+N_t}(x) \right] \tag{14}$$

The shape function of nodal displacements produced by Tchebychev radial point interpolation method can be ascertained as follows:

$$\boldsymbol{\Phi}^T(x) = \left[\phi_1(x) \ \phi_2(x) \cdots \phi_N(x) \right] \tag{15}$$

2.3 Governing equation of sandwich shell

According to FSDT and Donnel shell assumption, the displacement components of any point of each layer are expressed as [24]

$$\begin{cases} \overline{u}_i = u_i + z\psi_{xi} \\ \overline{v}_i = v_i + z\psi_{\theta i} & i = s, v, c \\ \overline{w}_i = w \end{cases} \tag{16}$$

where u_i, v_i and w denote the displacement components of middle surface of each layer in the x, θ and z directions, respectively. For the base layer and constraining layer, the shear rotations ψ_{xi} and $\psi_{\theta i}$ can be determined as follows:

$$\begin{cases} \psi_{xi} = -\frac{\partial w}{\partial x} \\ \psi_{\theta i} = -\frac{\partial w}{R_i \partial \theta} & i = s, c \end{cases} \tag{17}$$

where $R_i = R_{i0} + x\sin\alpha$.

The displacements of the viscoelastic layer can be ascertained as the following expression based on the displacement continuity conditions of interlayer.

$$u_v = \frac{1}{2}\left(u_s + u_c + \frac{h_s}{2}\psi_{xs} - \frac{h_c}{2}\psi_{xc} \right), \ \psi_{xv} = \frac{1}{h_v}\left(u_c - u_s - \frac{h_s}{2}\psi_{xs} - \frac{h_c}{2}\psi_{xc} \right)$$
$$v_v = \frac{1}{2}\left(v_s + v_c + \frac{h_s}{2}\psi_{\theta s} - \frac{h_c}{2}\psi_{\theta c} \right), \ \psi_{\theta v} = \frac{1}{h_v}\left(v_c - v_s - \frac{h_s}{2}\psi_{\theta s} - \frac{h_c}{2}\psi_{\theta c} \right) \tag{18}$$

Generally, the Young's modulus of the base layer and constraining layer is much larger than the that of viscoelastic core layer. Therefore, the former only considers flexural and axial deformations, and the latter only considers shear strains. Considering Eq. (18), the strains of the viscoelastic core layer are expressed as:

$$\gamma_{xz}^v = \frac{1}{h_v}(u_c - u_s) + c_x \frac{\partial w}{\partial x}$$
$$\gamma_{\theta z}^v = \left(\frac{1}{h_v} - \frac{\cos\alpha}{2R_v} \right)v_c - \left(\frac{1}{h_v} + \frac{\cos\alpha}{2R_v} \right)v_s + c_\theta \frac{\partial w}{\partial \theta} \tag{19}$$

where

$$c_x = \frac{h_s + h_c + 2h_v}{2h_v}$$
$$c_\theta = \left[\frac{1}{2h_v}\left(\frac{h_c}{R_c} + \frac{h_s}{R_s} \right) + \frac{1}{4R_v}\left(\frac{h_s\cos\alpha}{R_s} - \frac{h_c\cos\alpha}{R_c} + 4 \right) \right] \tag{20}$$

The shear stresses with regard to the viscoelastic core layer can be written as follows:

$$\tau_{xz}^v = G_v\gamma_{xz}^v \quad \tau_{\theta z}^v = G_v\gamma_{\theta z}^v \tag{21}$$

where G_v denotes shear modulus with regard to the viscoelastic core layer, which consists of real and imaginary parts.

$$G_v = G_r + iG_i \tag{22}$$

where G_r and G_i denote the real and imaginary parts of the above shear modulus G_v, respectively.

Meanwhile, the relationships between stress and strain of the base and constraining layers are written as follows:

$$\begin{bmatrix} \sigma_x^i \\ \sigma_\theta^i \\ \tau_{x\theta}^i \end{bmatrix} = \begin{bmatrix} Q_{11} & Q_{12} & 0 \\ Q_{12} & Q_{11} & 0 \\ 0 & 0 & Q_{66} \end{bmatrix} \begin{bmatrix} \varepsilon_x^i \\ \varepsilon_\theta^i \\ \gamma_{x\theta}^i \end{bmatrix} \quad i = s, c \tag{23}$$

where the stiffness coefficients Q_{mn} of the isotropic material are as

$$Q_{11} = \frac{E_i}{1 - \mu_i^2}, \quad Q_{12} = \frac{\mu_i E_i}{1 - \mu_i^2}, \quad Q_{66} = \frac{E_i}{2(1 + \mu_i)} \tag{24}$$

where E_i and μ_i denote Young's modulus and Poisson's ratios with regard to the base and constraining layers. The relationships between strain and displacement of the base and constraining layers can be determined as follows:

$$\varepsilon_x^i = \frac{\partial u_i}{\partial x} - z\frac{\partial^2 w}{\partial x^2}$$
$$\varepsilon_\theta^i = \frac{\sin\alpha}{R_i}u_i + \frac{1}{R_i}\frac{\partial v_i}{\partial\theta} + \frac{\cos\alpha}{R_i}w - z\frac{\sin\alpha}{R_i}\frac{\partial w}{\partial x} - \frac{z}{R_i^2}\frac{\partial^2 w}{\partial\theta^2}$$
$$\gamma_{x\theta}^i = \frac{1}{R_i}\frac{\partial u_i}{\partial\theta} + \frac{\partial v_i}{\partial x} - \frac{\sin\alpha}{R_i}v_i + 2z\frac{\sin\alpha}{R_i^2}\frac{\partial w}{\partial\theta} - \frac{2z}{R_i}\frac{\partial^2 w}{\partial x\partial\theta}$$

(25)

The above displacement components can be expanded as follows by introducing the meshfree TRPIM shape function.

$$u_s = \sum_{m=1}^{N}\sum_{n=0}^{M}\phi_m(x)\Big[\cos(n\theta)\tilde{U}_{mn}^s + \sin(n\theta)\overline{U}_{mn}^s\Big]e^{i\omega t}$$

$$v_s = \sum_{m=1}^{N}\sum_{n=0}^{M}\phi_m(x)\Big[\sin(n\theta)\tilde{V}_{mn}^s + \cos(n\theta)\overline{V}_{mn}^s\Big]e^{i\omega t}$$

$$u_c = \sum_{m=1}^{N}\sum_{n=0}^{M}\phi_m(x)\Big[\cos(n\theta)\tilde{U}_{mn}^c + \sin(n\theta)\overline{U}_{mn}^c\Big]e^{i\omega t}$$

(26)

$$v_c = \sum_{m=1}^{N}\sum_{n=0}^{M}\phi_m(x)\Big[\sin(n\theta)\tilde{V}_{mn}^c + \cos(n\theta)\overline{V}_{mn}^c\Big]e^{i\omega t}$$

$$w = \sum_{m=1}^{N}\sum_{n=0}^{M}\phi_m(x)\Big[\cos(n\theta)\tilde{W}_{mn} + \sin(n\theta)\overline{W}_{mn}\Big]e^{i\omega t}$$

where M and N represent the circumferential wave number and the node number which distributed in the meridional direction of shell, respectively. The symbols $\tilde{U}_{mn}^s$, $\tilde{V}_{mn}^s$, $\tilde{U}_{mn}^c$, $\tilde{V}_{mn}^c$, $\tilde{W}_{mn}$, $\overline{U}_{mn}^s$, $\overline{V}_{mn}^s$, $\overline{U}_{mn}^c$, $\overline{V}_{mn}^c$ and $\overline{W}_{mn}$ represent the displacement components with regard to node.

The strain energies of the sandwich shell can be described as follows:

$$U = \sum_{i=s}^{c}U_i + U_v \quad (i=s,c)$$

$$U_i = \frac{1}{2}\int_0^{2\pi}\int_0^L\int_{-h_i/2}^{h_i/2}\left(\sigma_x^i\varepsilon_x^i + \sigma_\theta^i\varepsilon_\theta^i + \tau_{x\theta}^i\gamma_{x\theta}^i\right)R_i\,dz\,dx\,d\theta; \quad U_v = \frac{1}{2}\int_0^{2\pi}\int_0^L\int_{-h_v/2}^{h_v/2}\left(\tau_{xz}^v\gamma_{xz}^v + \tau_{\theta z}^v\gamma_{\theta z}^v\right)R_v\,dz\,dx\,d\theta$$

(27)

The kinetic energies of the sandwich shell can be given as

$$T = \sum_{i=s}^{c}T_i + T_v(i=s,c)$$

$$T_i = \frac{\rho_i h_i}{2}\int_0^{2\pi}\int_0^L\left(\dot{u}_i^2 + \dot{v}_i^2 + \dot{w}^2\right)R_i\,dx\,d\theta; \quad T_v = \frac{\rho_v h_v}{2}\int_0^{2\pi}\int_0^L\dot{w}^2 R_v\,dx\,d\theta$$

(28)

where ρ_i ($i=s,v,c$) denotes the density of each layer.

The elastic energies stored in distributed springs of base and constraining layers can be given as

$$U_{BC} = \frac{1}{2}\sum_{i=s}^{c}\int_0^{2\pi}\left\{\begin{array}{l}\left[k_{u0}u_i^2 + k_{v0}v_i^2 + k_{w0}w^2 + K_{w0}(\partial w/\partial x)\right]_{x=0}\\ +\left[k_{u1}u_i^2 + k_{v1}v_i^2 + k_{w1}w^2 + K_{w1}(\partial w/\partial x)\right]_{x=L}\end{array}\right\}R_i\,d\theta(i=s,c)$$

(29)

The total Lagrangian energy function with regard to sandwich shell can be determined as follows:

$$L = T - U - U_{BC}$$

(30)

The extremum of the above Lagrangian energy function can be determined by the following derivative operation.

$$\frac{\partial L}{\partial q} = 0, \quad q = \tilde{U}_{mn}^s, \tilde{V}_{mn}^s, \tilde{U}_{mn}^c, \tilde{V}_{mn}^c, \tilde{W}_{mn}, \overline{U}_{mn}^s, \overline{V}_{mn}^s, \overline{U}_{mn}^c, \overline{V}_{mn}^c, \overline{W}_{mn}$$

(31)

Fig. 1 Diagram of sandwich
conical shell with viscoelastic core
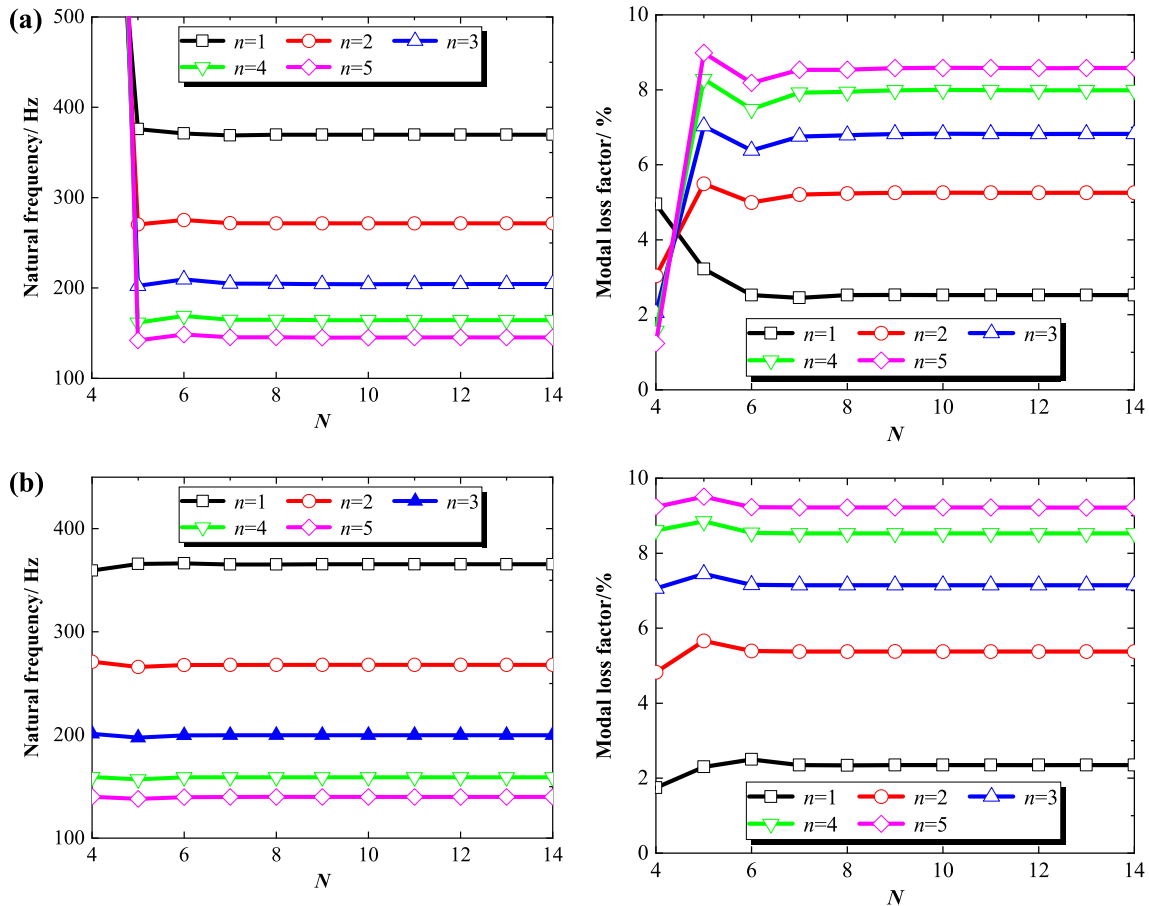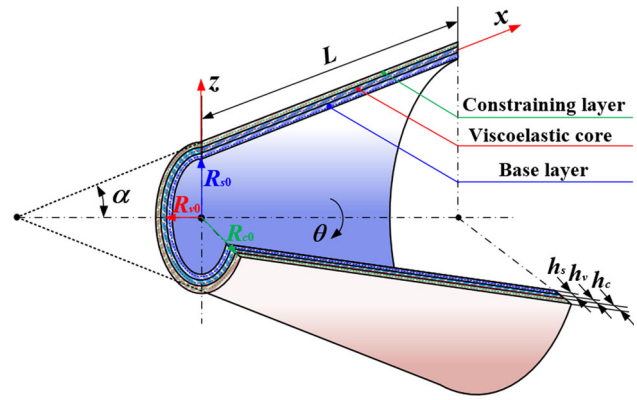
Fig. 2 Convergence of natural frequency and modal loss factor for a sandwich conical shell with different numbers of nodes N: **a** C–C and **b** S–S

Substituting Eqs. (27)–(30) into Eq. (31), following governing equations are obtained.

$$\left(K - \overline{\omega}^2 M\right)U_s = 0 \tag{32}$$

where U_s is the nodal displacement vector; K and M denote mass and stiffness matrices respectively, the concrete expression of the above matrices can be found in Appendices 1 and 2. From Eq. (32), the complex eigenvalues are obtained. The definitions of real frequency ω and modal loss factor η of sandwich shells are shown as follows:

$$\omega = \sqrt{\text{Re}(\overline{\omega}^2)} \tag{33}$$

$$\eta = \frac{\text{Im}(\overline{\omega}^2)}{\text{Re}(\overline{\omega}^2)} \tag{34}$$
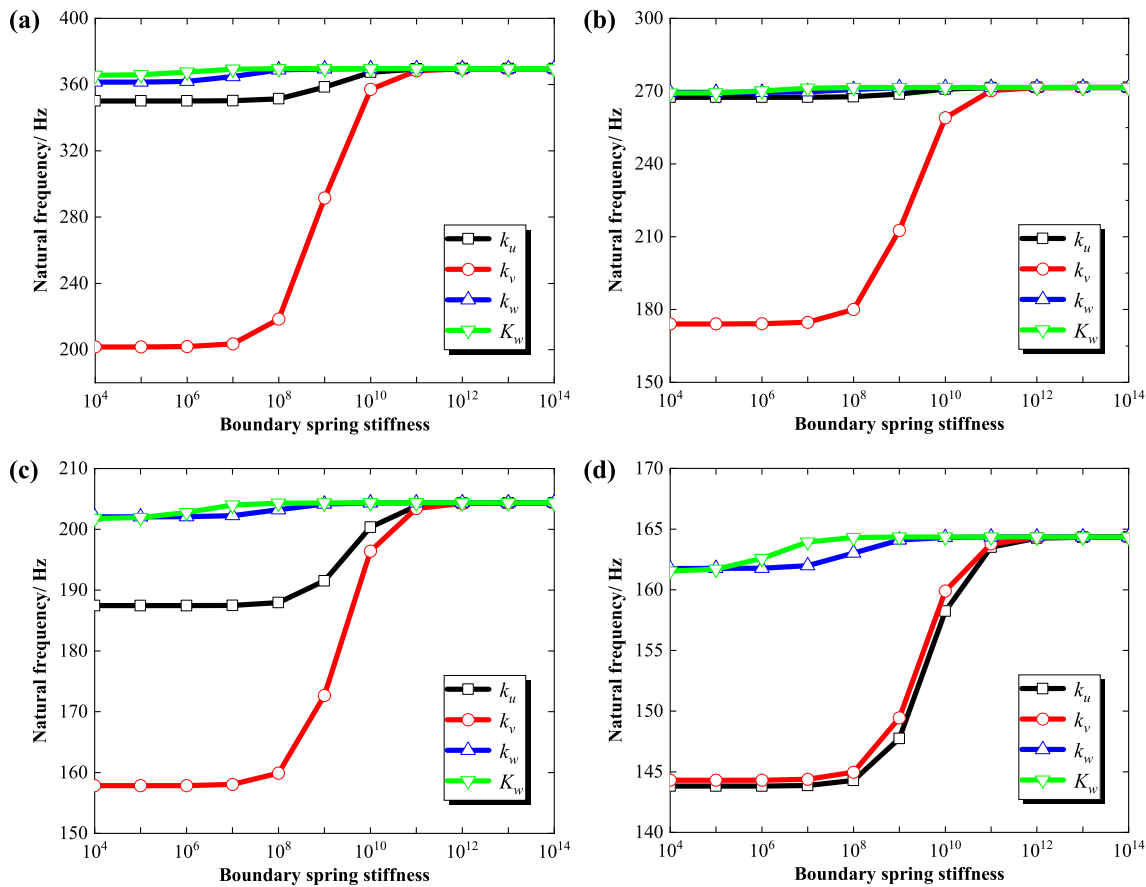
Fig. 3 Convergence of natural frequency for a sandwich conical shell with different boundary spring stiffnesses: **a** $n = 1$, **b** $n = 2$, **c** $n = 3$ and **d** $n = 4$

3 Numerical discussion

The validity including accuracy and reliability of the presented method is performed for demonstrating that it can be used to analyze the vibration and damping behaviors of sandwich shells including conical shell and cylindrical shell in this section.

Unless otherwise specified, the material parameters of sandwich shells in the following discussion are selected as: $E_s = E_c = 210$ GPa, $G_r = 8.582$ MPa, $G_i = 2.985$ MPa, $\mu_s = \mu_c = 0.3$, $\rho_s = \rho_c = 7850$ kg/m^3 and $\rho_v = 1340$ kg/m^3.

3.1 Convergence and verification analyses

The computational cost and accuracy of the meshfree numerical solution are influenced by the number of divided node in the solving domain. However, it is worth noting that the computational cost and accuracy exist certain contradiction. The above contradiction can be interpreted as the computational cost and accuracy increase with the number of divided node increased. The influence of divided node number N on the natural frequencies and modal loss factor of sandwich conical shell structure are investigated; the corresponding results can be found in Fig. 2. The geometric parameters of sandwich conical shell structure are defined as: $R_s = 1$ m, $L = 2$ m, $h_s = h_c = 2h_v = 0.02$ m and $\alpha = \pi/6$.

As shown in Fig. 2, the natural frequencies and modal loss factors of sandwich conical shell subjected to various boundary conditions have varying degree variation tendencies firstly and then remain unchanged with the number of divided node increased. The above results indicate that the proposed method has stable convergence in the process of analyzing the vibration and damping behaviors of sandwich shells under various boundary conditions.

According to the above discussion, the various boundary conditions of the proposed method are simulated by employing artificial spring technique. The crucial of artificial spring technique is select appropriate spring stiffness value in different directions. In order to determine the spring stiffness value of various boundary conditions, the effects of spring stiffness values on the natural frequencies and modal loss factors of sandwich shells including conical shell and cylindrical shell are discussed, the corresponding results are shown in Figs. 3 and 4. The geometric parameters used in this discussion can be found in Fig. 2. The left and right sides of sandwich shell structure are selected as elastic boundary and completely clamped boundary, respectively. The longitudinal mode number is selected as $m = 1$.
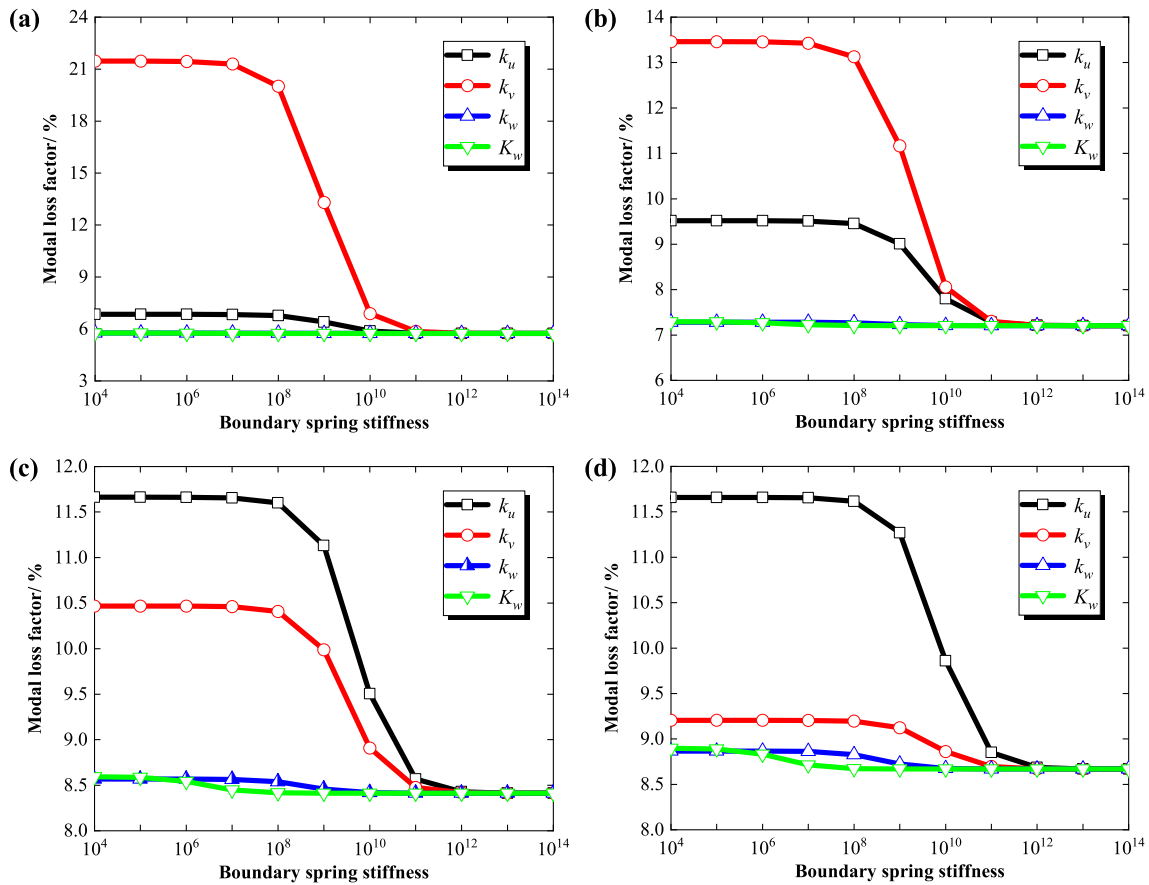
Fig. 4 Convergence of modal loss factor for a sandwich cylindrical shell with different boundary spring stiffnesses: **a** $n = 1$, **b** $n = 2$, **c** $n = 3$ and **d** $n = 4$

Table 1 Stiffness values for different boundary springs

B.C	Boundary spring stiffness value			
	$k_{u,}$	k_v	k_w	K_w
F	0	0	0	0
C	10^{14}	10^{14}	10^{14}	10^{14}
S	10^{14}	10^{14}	10^{14}	0
SD	0	10^{14}	10^{14}	0

As shown in Figs. 3 and 4, the natural frequencies and modal loss factors of sandwich shells have opposite variation tendencies firstly and then keep constant with the spring stiffness values of different directions increased. The above results indicate that the solution of natural frequencies and modal loss factors of sandwich shells reach stable convergence when spring stiffness values increase to 10^{13}.

According to the above discussion, the values of spring stiffness subjected to various boundary condition are ascertained in Table 1. It is necessary to point out that F and C denote free and clamped boundary conditions, respectively; S and SD represent simply supported and shear diaphragm boundary conditions, respectively.

Then, the validation of the presented method is performed by comparing the results calculated by the proposed method with the corresponding results from the existing literatures. The material geometric parameters are selected as: $E_s = E_c = 70$ GPa, $G_v = 0.896(1 + i0.9683)$ MPa, $\mu_s = \mu_c = 0.3$, $\rho_s = \rho_c = 2700$ kg/m^3, $\rho_v = 999$ kg/m^3, $h_s = h_c = 2h_v = 0.02$ m, $R_s = 1$ m, $L = 0.5$ m. The comparison results of natural frequencies of sandwich cylindrical shell subjected to different boundary conditions are shown in Table 2. The material geometric parameters are consistent with Table 2 except for the following geometric parameters $L = R_s = 3$ m, $h_s = h_c$. The two sides of the shell are selected as simply supported boundary condition, and the axial wave number is chosen as $m = 1$. The comparison results of natural frequencies of sandwich cylindrical shell under various thickness ratios can be found in Table 3. As shown in Tables 2 and 3, it is not hard to see that the comparison results between proposed method and the existing literatures have good consistency.

Table 2 Comparison of natural frequencies for a sandwich cylindrical shell with various boundary conditions

B.C	n	m = 1			m = 2			m = 3		
		Ref. [40]	Present	Diff (%)	Ref. [40]	Present	Diff (%)	Ref. [40]	Present	Diff (%)
C–C	1	873.13	873.128	0.0002	1387.56	1387.555	0.0004	2399.36	2398.975	0.0160
	2	821.85	821.847	0.0004	1389.00	1388.991	0.0006	2406.83	2406.467	0.0151
	3	764.95	764.945	0.0007	1392.36	1392.345	0.0011	2420.62	2420.307	0.0129
	4	718.50	718.493	0.0010	1399.03	1399.003	0.0019	2441.10	2440.841	0.0106
	5	689.18	689.173	0.0010	1410.73	1410.701	0.0021	2468.48	2468.286	0.0079
C–S	1	820.19	820.185	0.0006	1209.98	1209.971	0.0007	2106.02	2105.925	0.0045
	2	765.25	765.244	0.0008	1210.28	1210.272	0.0007	2114.57	2114.485	0.0040
	3	702.95	702.942	0.0011	1212.62	1212.614	0.0005	2129.60	2129.536	0.0030
	4	650.64	650.635	0.0008	1218.66	1218.652	0.0007	2151.54	2151.493	0.0022
	5	616.30	616.296	0.0006	1230.27	1230.263	0.0006	2180.73	2180.719	0.0005
C–SD	1	799.83	799.824	0.0008	1209.68	1209.673	0.0006	2103.43	2103.329	0.0048
	2	757.92	757.918	0.0003	1210.27	1210.266	0.0003	2113.14	2113.049	0.0043
	3	702.45	702.442	0.0011	1212.49	1212.487	0.0002	2128.99	2128.921	0.0032
	4	649.75	649.743	0.0011	1218.29	1218.282	0.0007	2151.28	2151.243	0.0017
	5	611.95	611.945	0.0008	1229.83	1229.819	0.0009	2180.62	2180.607	0.0006
C–F	1	669.29	669.283	0.0010	861.71	861.686	0.0028	1389.70	1389.691	0.0006
	2	519.66	519.647	0.0025	850.84	850.818	0.0026	1396.88	1396.866	0.0010
	3	406.55	406.536	0.0034	834.00	833.980	0.0024	1409.84	1409.820	0.0014
	4	333.28	333.261	0.0057	814.00	813.983	0.0021	1429.37	1429.339	0.0022
	5	295.42	295.406	0.0047	798.32	798.312	0.0010	1456.46	1456.428	0.0022

Table 3 Comparison of natural frequencies for a sandwich cylindrical shell with various thickness ratios

h_s/R_s	h_v/h_s	Circumferential wave number								
		1			2			3		
		Ref. [40]	Present	Diff (%)	Ref. [40]	Present	Diff (%)	Ref. [40]	Present	Diff (%)
1/20	1	219.06	219.061	− 0.0005	175.10	175.101	− 0.0006	146.60	146.603	− 0.0020
	2	200.92	200.915	0.0025	161.71	161.712	− 0.0012	135.60	135.595	0.0037
	3	185.83	185.830	0.0000	150.52	150.519	0.0007	126.46	126.462	− 0.0016
	4	173.05	173.046	0.0023	140.97	140.971	− 0.0007	118.71	118.713	− 0.0025
1/60	1	220.90	220.902	− 0.0009	171.22	171.221	− 0.0006	133.74	133.740	0.0000
	2	204.91	204.912	− 0.0010	159.36	159.358	0.0013	124.56	124.560	0.0000
	3	191.65	191.654	− 0.0021	149.52	149.519	0.0007	116.98	116.984	− 0.0034
	4	180.43	180.426	0.0022	141.18	141.181	− 0.0007	110.59	110.587	0.0027
1/100	1	221.66	221.654	0.0027	171.17	171.156	0.0082	132.69	132.681	0.0068
	2	206.11	206.108	0.0010	159.54	159.538	0.0013	123.70	123.693	0.0057
	3	193.24	193.241	− 0.0005	149.92	149.919	0.0007	116.29	116.284	0.0052
	4	182.36	182.362	− 0.0011	141.78	141.781	− 0.0007	110.04	110.037	0.0027

Table 4 Dimensionless frequencies for a sandwich conical shell with various semi-vertex angles ($m = 1$)

α	n	B.C							
		C–C	C–S	C–SD	S–S	S–SD	SD–SD	F–C	F–S
0	1	0.0439	0.0437	0.0433	0.0435	0.0430	0.0336	0.0286	0.0285
	2	0.0345	0.0341	0.0340	0.0338	0.0337	0.0300	0.0178	0.0175
	3	0.0276	0.0271	0.0263	0.0265	0.0258	0.0254	0.0121	0.0118
	4	0.0233	0.0226	0.0214	0.0219	0.0208	0.0198	0.0096	0.0094
$\pi/6$	1	0.0323	0.0314	0.0294	0.0314	0.0293	0.0258	0.0286	0.0282
	2	0.0274	0.0267	0.0265	0.0265	0.0263	0.0216	0.0198	0.0195
	3	0.0230	0.0223	0.0222	0.0219	0.0218	0.0210	0.0141	0.0138
	4	0.0199	0.0190	0.0185	0.0185	0.0179	0.0176	0.0110	0.0107
$\pi/4$	1	0.0251	0.0240	0.0220	0.0240	0.0219	0.0197	0.0234	0.0227
	2	0.0220	0.0210	0.0206	0.0209	0.0204	0.0175	0.0173	0.0169
	3	0.0189	0.0180	0.0180	0.0177	0.0176	0.0162	0.0127	0.0124
	4	0.0168	0.0158	0.0155	0.0153	0.0150	0.0148	0.0102	0.0098
$\pi/3$	1	0.0178	0.0166	0.0151	0.0165	0.0149	0.0135	0.0167	0.0159
	2	0.0160	0.0148	0.0144	0.0146	0.0142	0.0126	0.0129	0.0124
	3	0.0143	0.0131	0.0131	0.0127	0.0127	0.0113	0.0099	0.0095
	4	0.0132	0.0119	0.0119	0.0114	0.0113	0.0112	0.0084	0.0080

3.2 Parametric analysis

According to the above convergence and verification analyses, the validation including accuracy and stability of the proposed approach is verified. The vibration and damping behaviors of sandwich shells including shell conical and cylindrical shell are investigated by analyzing the influences of some parameters on the natural frequencies and modal loss factor in this section.

First of all, the effect of semi-vertex angle on the natural frequencies (dimensionless frequency) and modal loss factors of sandwich conical shell are investigated; the corresponding results can be seen in Table 4 and Fig. 5, respectively. The definition of dimensionless frequency is shown as: $\Omega = \omega R_s^2 \sqrt{\rho_s/E_s h^2}$, the total thickness of sandwich conical shell is $h = h_s + h_v + h_c$. The geometric parameters are selected as: $R_s = 1$ m, $L = 1$ m and $h_s = h_c = 2h_v = 0.02$ m.

From Table 4 and Fig. 5, it is easy to find that the natural frequencies and modal loss factors have opposite variation tendencies with the company of semi-vertex angle increased, the former decreases and the latter increase, respectively. Meanwhile, it is necessary to point out that the variation tendency of modal loss factors is remarkable when the semi-vertex angle increases to 70°.

Subsequently, the effects of thickness of viscoelastic core layer on the natural frequencies and modal loss factors of sandwich conical shell and cylindrical shell are investigated; the corresponding results are shown in Table 5 and Fig. 6. The above natural frequencies are nondimensionalized by means of $\Omega = \omega R_s^2 \sqrt{\rho_s/E_s h^2}$; the definition of thickness ratio of sandwich conical shell is
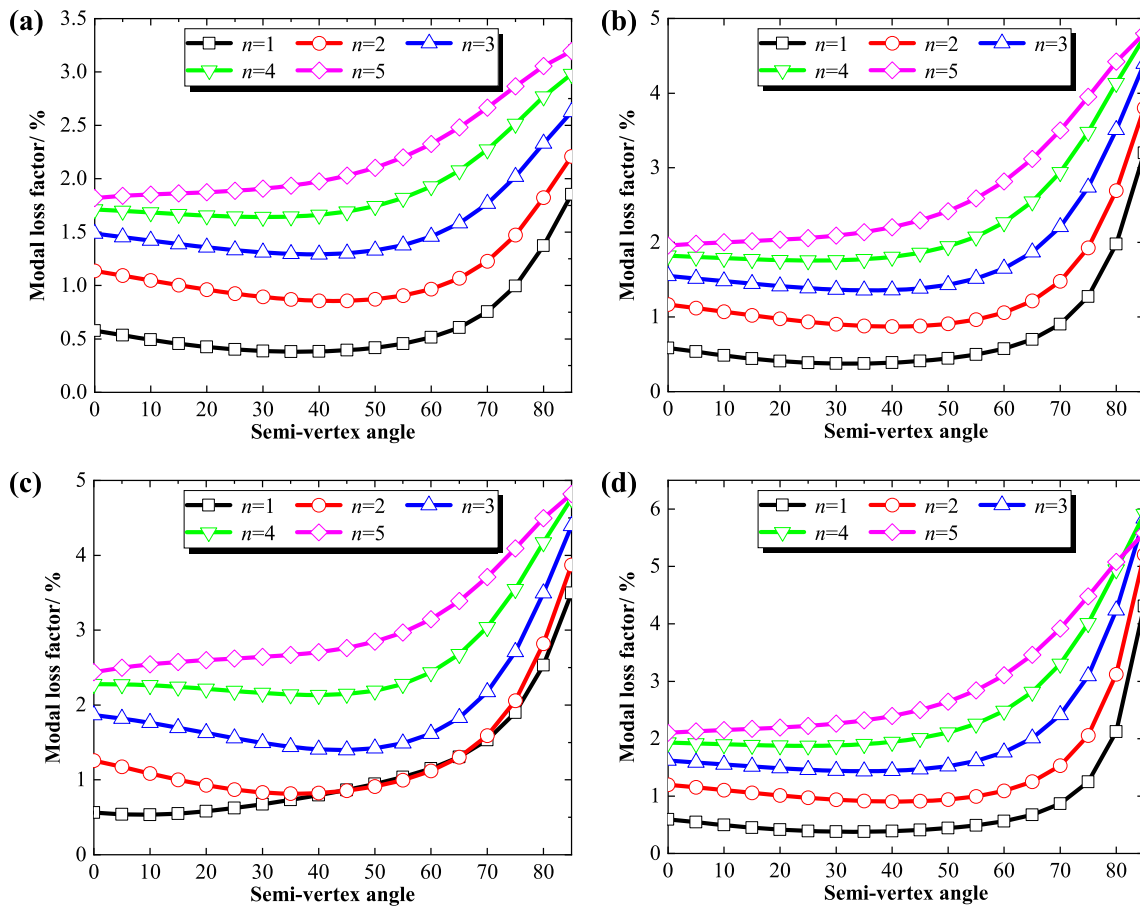
Fig. 5 Variation of modal loss factors for a sandwich conical shell with various semi-vertex angles ($m = 1$): **a** C–C, **b** C–S, **c** C–SD and **d** S–S

set as h_v/h. The thickness of base layer is consistent with the thickness of constraining layer. The geometric parameters is selected as: $R_s = 1$ m, $L = 2$ m, $\alpha = \pi/6$ and $h = 0.05$ m. As shown in Table 5, it is easy to see that the thickness ratio has important effect in the vibration characteristics of sandwich conical shell. The model parameters of Fig. 6 are the same as Table 5 except the total thickness of conical shell is chosen as $h = 0.1$ m. From Fig. 6, the natural frequencies decrease with the thickness of viscoelastic core layer increased. However, the modal loss factors decrease firstly and then increase with the thickness of viscoelastic core layer increased.

Then, the influences of circumferential wave number on the natural frequencies and modal loss factors of sandwich shells including conical shell and cylindrical shell subjected to various boundary conditions are discussed; the corresponding results can be seen in Fig. 7. The geometric parameters of sandwich shells are selected as: $R_s = 1$ m, $L = 2$ m and $h_s = h_c = h_v = 0.02$ m. From Fig. 7, it is easy to see that the natural frequencies and modal loss factors of sandwich cylindrical shell subjected to various boundary conditions attain minimum and maximum values when the circumferential wave number is set as 4. The natural frequencies and modal loss factors of sandwich conical shell subjected to C–SD and S–SD boundary conditions get minimum and maximum values when the circumferential wave number is set as 5. When sandwich conical shell under the C–C, C–S and S–S boundary conditions, the above corresponding circumferential wave number is set as 6.

Fourthly, the influences of material loss factor G_i/G_r of viscoelastic material layer on modal loss factors of sandwich shells are researched; the corresponding results are shown in Fig. 8. The geometric parameters are consistent with the corresponding parameters come from Fig. 7 except for the real part of shear modulus is chosen as $G_r = 8.582$ MPa. As shown in Fig. 8, the modal loss factors increased by means of linear with the material loss factor G_i/G_r increased. The influence of material loss factor on modal loss factors of sandwich shells under C–SD boundary condition is much larger than that of sandwich shells under C–C boundary condition.

Finally, the effects of various geometric parameters, circumferential wave numbers and boundary conditions on natural frequencies of sandwich shells including cylindrical shell and conical shell are performed; the corresponding results of cylindrical shell and conical shell can be found in Table 6 and Table 7. The geometric parameters are chosen as: $R_s = 1$ m, $h_v = 0.02$ m and $h_s = h_c = 0.01$ m. The dimensionless definition of natural frequencies can be expressed as $\Omega = \omega R_s^2 \sqrt{\rho_s/E_s h^2}$. As shown in Tables 6 and 7, the structure length has significantly effect on the natural frequencies of sandwich shells compared with circumferential wave

Table 5 Dimensionless frequencies for a sandwich conical shell with various thickness ratios ($m = 1$)

| h_v/h	n	B.C							
		C–C	C–S	C–SD	S–S	S–SD	SD–SD	F–C	F–S
0.1	1	0.0249	0.0246	0.0230	0.0246	0.0230	0.0196	0.0211	0.0210
	2	0.0183	0.0181	0.0179	0.0180	0.0178	0.0176	0.0125	0.0123
	3	0.0139	0.0137	0.0127	0.0135	0.0125	0.0121	0.0081	0.0081
	4	0.0115	0.0112	0.0099	0.0110	0.0097	0.0092	0.0072	0.0071
0.2	1	0.0225	0.0222	0.0208	0.0222	0.0207	0.0171	0.0191	0.0190
	2	0.0165	0.0164	0.0162	0.0163	0.0161	0.0159	0.0112	0.0112
	3	0.0124	0.0123	0.0113	0.0121	0.0112	0.0108	0.0072	0.0071
	4	0.0100	0.0098	0.0086	0.0097	0.0084	0.0079	0.0059	0.0058
0.3	1	0.0221	0.0219	0.0204	0.0219	0.0204	0.0168	0.0188	0.0187
	2	0.0162	0.0161	0.0159	0.0161	0.0159	0.0157	0.0111	0.0110
	3	0.0122	0.0120	0.0111	0.0119	0.0110	0.0106	0.0070	0.0069
	4	0.0097	0.0095	0.0083	0.0094	0.0082	0.0077	0.0055	0.0055
0.4	1	0.0217	0.0215	0.0200	0.0215	0.0200	0.0165	0.0185	0.0185
	2	0.0159	0.0158	0.0156	0.0158	0.0156	0.0154	0.0109	0.0108
	3	0.0119	0.0118	0.0108	0.0117	0.0108	0.0104	0.0068	0.0067
	4	0.0094	0.0093	0.0081	0.0092	0.0080	0.0074	0.0052	0.0051
0.5	1	0.0211	0.0209	0.0195	0.0209	0.0195	0.0163	0.0181	0.0181
	2	0.0155	0.0154	0.0153	0.0154	0.0152	0.0151	0.0106	0.0106
	3	0.0115	0.0115	0.0196	0.0114	0.0105	0.0101	0.0066	0.0065
	4	0.0091	0.0090	0.0078	0.0089	0.0077	0.0072	0.0049	0.0049
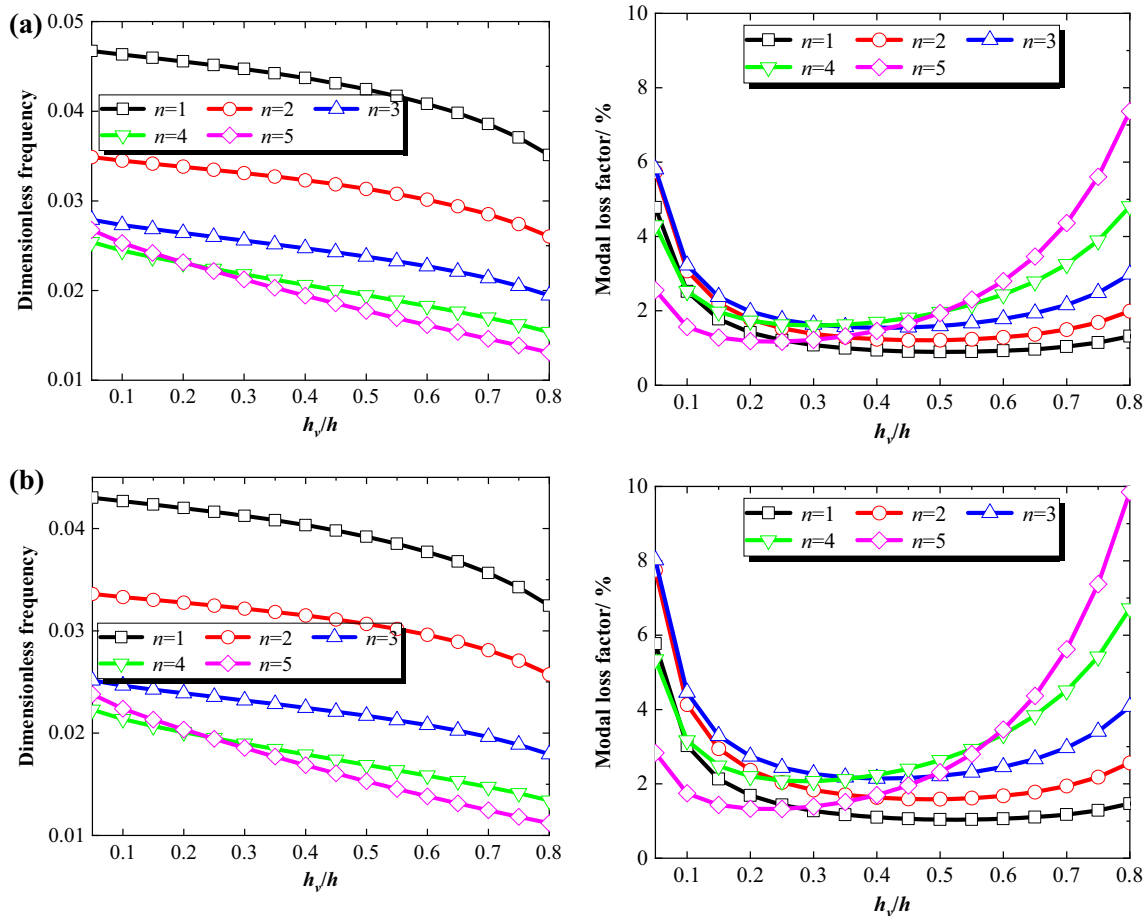
Fig. 6 Variation of dimensionless frequency and modal loss factor for a sandwich conical shell with various thickness ratios ($m = 1$): **a** C–C and **b** C–SD
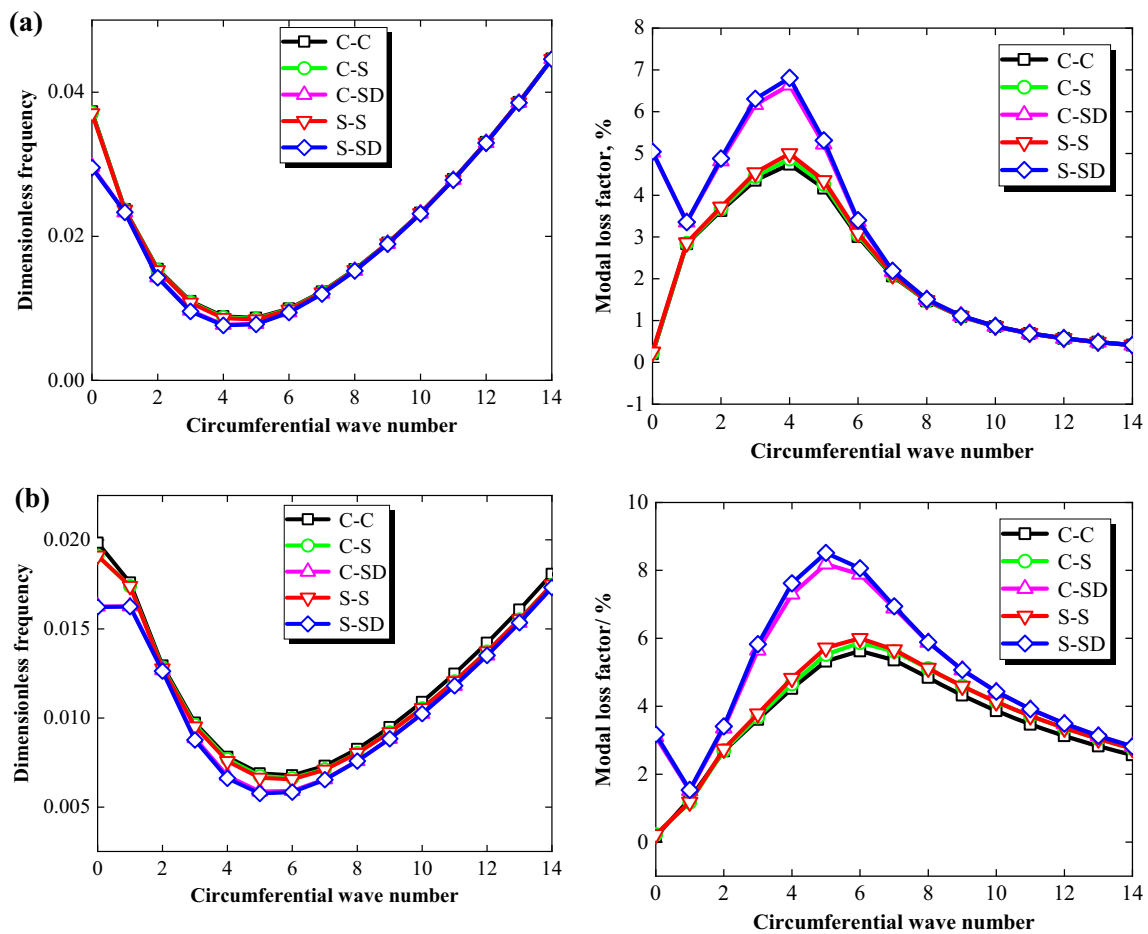
Fig.7 Variation of dimensionless frequency and modal loss factor for a sandwich shell according to circumferential wave number ($m = 1$): **a** cylindrical shell and **b** conical shell ($\alpha = \pi/6$)

numbers and boundary conditions. According to the variation tendencies of the above natural frequencies, it can conclude that the increase of structure length will result in the decrease of stiffness of sandwich shells.

4 Conclusion

A meshless method is proposed to investigate the vibration and damping characteristics of sandwich shells including cylindrical shell and conical shell. The sandwich shells are made up of three layers including base layer, viscoelastic core layer and constraining layer. The theoretical modeling of sandwich shells is deduced by employing the energy principle in framework of FSDT and Donnel shell hypothesis. The displacement components of arbitrary point locate at the sandwich shell are expanded by employing the circumferential Fourier series and the meridional direction meshfree TRPIM shape function. The convergence and validation including accuracy and stability of the proposed method are verified by comparing the results calculated by the presented approach with the corresponding results of existing literatures. Based on the above proposed method, the vibration and damping behaviors analysis of sandwich shells are carried out by investigating the influences of some parameters including geometric dimensions, material parameters and circumferential wave numbers on the natural frequencies and modal loss factors of sandwich shells. Some representative conclusions are shown as follows:

(1) The influences of semi-vertex angle on the natural frequencies and modal loss factors of sandwich conical shell structure are opposite. The increase of semi-vertex angle leads to the decrease and increase of natural frequencies and modal loss factors, respectively.
(2) The thickness of viscoelastic core layer has important effects on the natural frequencies and modal loss factors of sandwich shell structure.
(3) The natural frequencies and modal loss factors of sandwich shell structure exist the extreme value phenomenon under the effects of circumferential waver number and boundary condition.
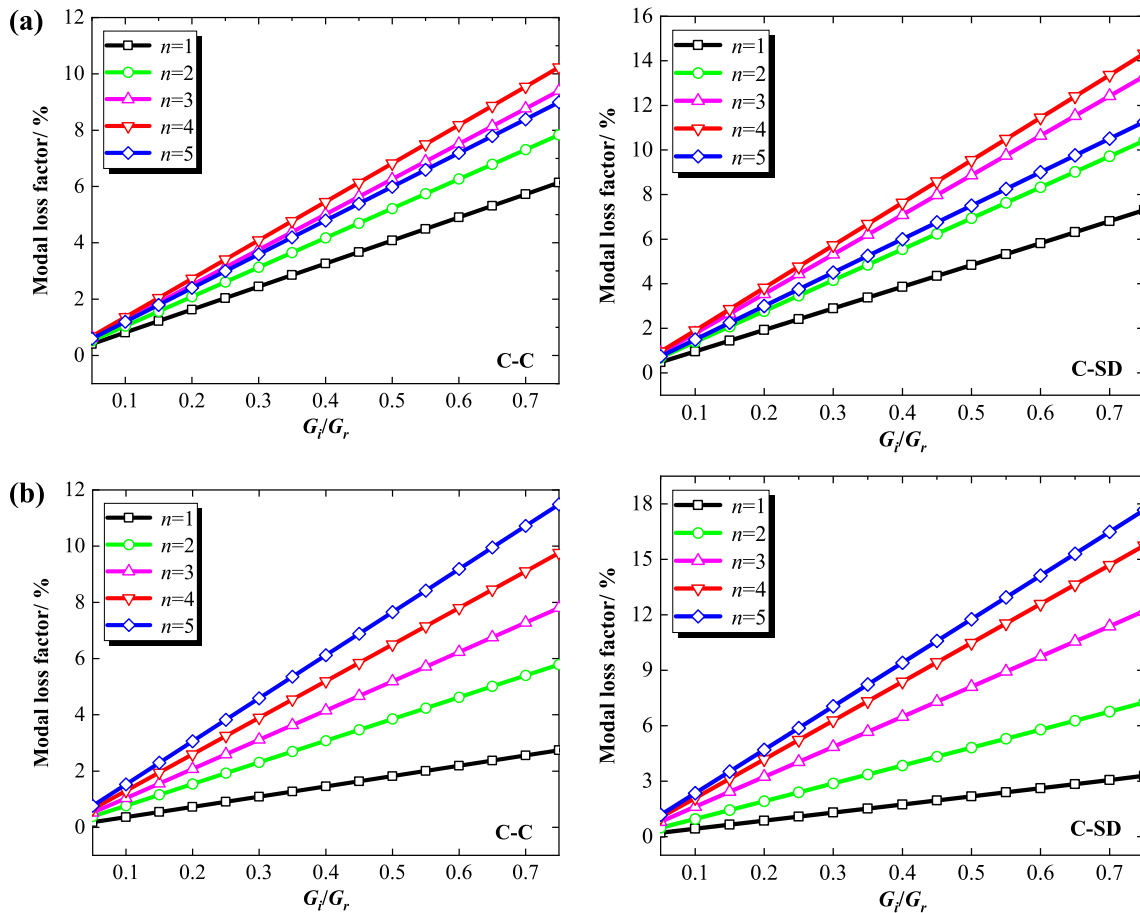
Fig. 8 Variation of modal loss factor for a sandwich shell according to material loss factor of viscoelastic material layer ($m = 1$): **a** cylindrical shell and **b** conical shell ($\alpha = \pi/6$)

(4)   The material loss factor G_i/G_r of viscoelastic material layer and the modal loss factors of sandwich conical shell structure are positively correlated.

Data Availability   The data that support the findings of this study are available within the article. The manuscript has associated data in a data repository.

Declarations

Appendix 1. The components of the complex stiffness matrix K

$$A_{inm} = Q_{nm}h_i$$
$$D_{inm} = \frac{1}{12}Q_{nm}h_i^3 \quad i = s, c \quad m, n = 1, 2, 6, \quad R_{i1} = R_{i0} + L\sin\alpha, \quad i = s, c$$
$$D_v = G_v h_v$$

$$\boldsymbol{K} = \boldsymbol{K}_c + \boldsymbol{K}_{bl} + \boldsymbol{K}_{br}$$

$$-n = 0$$

Table 6 Dimensionless frequencies for a sandwich cylindrical shell with various length ratios ($m = 1$)

L/R_s	n	B.C							
		C–C	C–S	C–SD	S–S	S–SD	SD–SD	F–C	F–S
0.5	1	0.0379	0.0373	0.0362	0.0369	0.0358	0.0240	0.0317	0.0315
	2	0.0351	0.0344	0.0340	0.0339	0.0335	0.0334	0.0244	0.0241
	3	0.0317	0.0309	0.0308	0.0302	0.0302	0.0302	0.0187	0.0184
	4	0.0286	0.0276	0.0276	0.0268	0.0268	0.0268	0.0148	0.0144
1	1	0.0330	0.0329	0.0326	0.0329	0.0325	0.0240	0.0219	0.0218
	2	0.0257	0.0256	0.0255	0.0255	0.0254	0.0254	0.0134	0.0133
	3	0.0201	0.0199	0.0194	0.0198	0.0192	0.0189	0.0088	0.0087
	4	0.0163	0.0161	0.0152	0.0159	0.0149	0.0142	0.0064	0.0063
2	1	0.0231	0.0230	0.0227	0.0230	0.0227	0.0227	0.0110	0.0110
	2	0.0148	0.0148	0.0138	0.0147	0.0137	0.0130	0.0055	0.0055
	3	0.0103	0.0102	0.0091	0.0102	0.0090	0.0078	0.0033	0.0033
	4	0.0077	0.0077	0.0066	0.0076	0.0065	0.0054	0.0029	0.0029
5	1	0.0096	0.0096	0.0085	0.0096	0.0084	0.0074	0.0028	0.0028
	2	0.0051	0.0051	0.0041	0.0050	0.0041	0.0031	0.0022	0.0022
	3	0.0032	0.0032	0.0025	0.0031	0.0025	0.0023	0.0014	0.0014
	4	0.0028	0.0028	0.0025	0.0028	0.0025	0.0020	0.0013	0.0012

Table 7 Dimensionless frequencies for a sandwich conical shell with various length ratios ($m = 1$, $\alpha = \pi/6$)

L/R_s	n	B.C							
		C–C	C–S	C–SD	S–S	S–SD	SD–SD	F–C	F–S
0.5	1	0.0301	0.0289	0.0274	0.0287	0.0271	0.0186	0.0275	0.0270
	2	0.0284	0.0272	0.0264	0.0269	0.0260	0.0249	0.0227	0.0223
	3	0.0263	0.0251	0.0248	0.0246	0.0243	0.0241	0.0182	0.0178
	4	0.0242	0.0229	0.0229	0.0222	0.0222	0.0222	0.0148	0.0143
1	1	0.0237	0.0233	0.0218	0.0233	0.0217	0.0193	0.0215	0.0213
	2	0.0201	0.0199	0.0197	0.0199	0.0197	0.0161	0.0149	0.0148
	3	0.0166	0.0164	0.0163	0.0163	0.0162	0.0161	0.0104	0.0103
	4	0.0139	0.0136	0.0132	0.0135	0.0130	0.0128	0.0077	0.0076
2	1	0.0169	0.0168	0.0156	0.0168	0.0156	0.0132	0.0145	0.0145
	2	0.0124	0.0123	0.0122	0.0123	0.0122	0.0121	0.0085	0.0085
	3	0.0092	0.0091	0.0084	0.0091	0.0084	0.0081	0.0052	0.0052
	4	0.0072	0.0071	0.0062	0.0071	0.0061	0.0057	0.0038	0.0038
5	1	0.0088	0.0088	0.0086	0.0088	0.0086	0.0084	0.0079	0.0079
	2	0.0054	0.0054	0.0049	0.0054	0.0048	0.0047	0.0037	0.0037
	3	0.0037	0.0037	0.0029	0.0037	0.0028	0.0026	0.0021	0.0021
	4	0.0028	0.0028	0.0022	0.0028	0.0022	0.0020	0.0019	0.0019

$$
\boldsymbol{K}_{bl} = \mathrm{diag}\Big[k_{u0}\boldsymbol{\Phi}^T\boldsymbol{\Phi}R_{s0} \quad k_{v0}\boldsymbol{\Phi}^T\boldsymbol{\Phi}R_{s0} \quad k_{u0}\boldsymbol{\Phi}^T\boldsymbol{\Phi}R_{c0} \quad k_{v0}\boldsymbol{\Phi}^T\boldsymbol{\Phi}R_{c0}
$$

$$
k_{w0}\boldsymbol{\Phi}^T\boldsymbol{\Phi}(R_{s0}+R_{c0}) + K_{w0}\frac{\partial\boldsymbol{\Phi}^T}{\partial x}\frac{\partial\boldsymbol{\Phi}}{\partial x}(R_{s0}+R_{c0}) \Big]_{x=0}
$$

$$
\boldsymbol{K}_{br} = \mathrm{diag}\Big[k_{u1}\boldsymbol{\Phi}^T\boldsymbol{\Phi}R_{s1} \quad k_{v1}\boldsymbol{\Phi}^T\boldsymbol{\Phi}R_{s1} \quad k_{u1}\boldsymbol{\Phi}^T\boldsymbol{\Phi}R_{c1} \quad k_{v1}\boldsymbol{\Phi}^T\boldsymbol{\Phi}R_{c1}
$$

$$
k_{w1}\boldsymbol{\Phi}^T\boldsymbol{\Phi}(R_{s1}+R_{c1}) + K_{w1}\frac{\partial\boldsymbol{\Phi}^T}{\partial x}\frac{\partial\boldsymbol{\Phi}}{\partial x}(R_{s1}+R_{c1}) \Big]_{x=L}
$$

$$
\boldsymbol{K}_c = \int_0^L \begin{bmatrix} k_{11} & k_{12} & \cdots & k_{15} \\ k_{12}^T & k_{22} & \cdots & k_{25} \\ \vdots & \vdots & \ddots & \vdots \\ k_{15}^T & k_{25}^T & \cdots & k_{55} \end{bmatrix} dx
$$

$$k_{11} = \left(A_{s11} \frac{\partial \boldsymbol{\Phi}^T}{\partial x} \frac{\partial \boldsymbol{\Phi}}{\partial x} + \frac{A_{s22} \sin^2 \alpha}{R_s^2} \boldsymbol{\Phi}^T \boldsymbol{\Phi} + \frac{A_{s12} \sin \alpha}{R_s} \frac{\partial \boldsymbol{\Phi}^T}{\partial x} \boldsymbol{\Phi} + \frac{A_{s12} \sin \alpha}{R_s} \boldsymbol{\Phi}^T \frac{\partial \boldsymbol{\Phi}}{\partial x} \right) R_s + \frac{D_v}{h_v^2} \boldsymbol{\Phi}^T \boldsymbol{\Phi} R_v$$

$$k_{13} = -\frac{D_v}{h_v^2} \boldsymbol{\Phi}^T \boldsymbol{\Phi} R_v$$

$$k_{15} = \left(\frac{A_{s12} \cos \alpha}{R_s} \frac{\partial \boldsymbol{\Phi}^T}{\partial x} \boldsymbol{\Phi} + \frac{A_{s22} \sin \alpha \cos \alpha}{R_s^2} \boldsymbol{\Phi}^T \boldsymbol{\Phi} \right) R_s - \frac{D_v c_x}{h_v} \boldsymbol{\Phi}^T \frac{\partial \boldsymbol{\Phi}}{\partial x} R_v$$

$$k_{22} = \left(A_{s66} \frac{\partial \boldsymbol{\Phi}^T}{\partial x} \frac{\partial \boldsymbol{\Phi}}{\partial x} + \frac{A_{s66} \sin^2 \alpha}{R_s^2} \boldsymbol{\Phi}^T \boldsymbol{\Phi} - \frac{A_{s66} \sin \alpha}{R_s} \frac{\partial \boldsymbol{\Phi}^T}{\partial x} \boldsymbol{\Phi} - \frac{A_{s66} \sin \alpha}{R_s} \boldsymbol{\Phi}^T \frac{\partial \boldsymbol{\Phi}}{\partial x} \right) R_s$$
$$+ D_v \left(\frac{1}{h_v} + \frac{\cos \alpha}{2R_v} \right)^2 \boldsymbol{\Phi}^T \boldsymbol{\Phi} R_v$$

$$k_{24} = -D_v \left(\frac{1}{h_v} - \frac{\cos \alpha}{2R_v} \right) \left(\frac{1}{h_v} + \frac{\cos \alpha}{2R_v} \right) \boldsymbol{\Phi}^T \boldsymbol{\Phi} R_v$$

$$k_{33} = \left(A_{c11} \frac{\partial \boldsymbol{\Phi}^T}{\partial x} \frac{\partial \boldsymbol{\Phi}}{\partial x} + \frac{A_{c22} \sin^2 \alpha}{R_c^2} \boldsymbol{\Phi}^T \boldsymbol{\Phi} + \frac{A_{c12} \sin \alpha}{R_c} \frac{\partial \boldsymbol{\Phi}^T}{\partial x} \boldsymbol{\Phi} + \frac{A_{c12} \sin \alpha}{R_c} \boldsymbol{\Phi}^T \frac{\partial \boldsymbol{\Phi}}{\partial x} \right) R_c + \frac{D_v}{h_v^2} \boldsymbol{\Phi}^T \boldsymbol{\Phi} R_v$$

$$k_{35} = \left(\frac{A_{c12} \cos \alpha}{R_c} \frac{\partial \boldsymbol{\Phi}^T}{\partial x} \boldsymbol{\Phi} + \frac{A_{c22} \sin \alpha \cos \alpha}{R_c^2} \boldsymbol{\Phi}^T \boldsymbol{\Phi} \right) R_c + \frac{D_v c_x}{h_v} \boldsymbol{\Phi}^T \frac{\partial \boldsymbol{\Phi}}{\partial x} R_v$$

$$k_{44} = \left(A_{c66} \frac{\partial \boldsymbol{\Phi}^T}{\partial x} \frac{\partial \boldsymbol{\Phi}}{\partial x} + \frac{A_{c66} \sin^2 \alpha}{R_c^2} \boldsymbol{\Phi}^T \boldsymbol{\Phi} - \frac{A_{c66} \sin \alpha}{R_c} \frac{\partial \boldsymbol{\Phi}^T}{\partial x} \boldsymbol{\Phi} - \frac{A_{c66} \sin \alpha}{R_c} \boldsymbol{\Phi}^T \frac{\partial \boldsymbol{\Phi}}{\partial x} \right) R_c$$
$$+ D_v \left(\frac{1}{h_v} - \frac{\cos \alpha}{2R_v} \right)^2 \boldsymbol{\Phi}^T \boldsymbol{\Phi} R_v$$

$$k_{55} = \left(\begin{array}{l} D_{s11} \frac{\partial^2 \boldsymbol{\Phi}^T}{\partial x^2} \frac{\partial^2 \boldsymbol{\Phi}}{\partial x^2} + \frac{D_{s22} \sin^2 \alpha}{R_s^2} \frac{\partial \boldsymbol{\Phi}^T}{\partial x} \frac{\partial \boldsymbol{\Phi}}{\partial x} + \frac{A_{s22} \cos^2 \alpha}{R_s^2} \boldsymbol{\Phi}^T \boldsymbol{\Phi} \\ + \frac{D_{s12} \sin \alpha}{R_s} \frac{\partial^2 \boldsymbol{\Phi}^T}{\partial x^2} \frac{\partial \boldsymbol{\Phi}}{\partial x} + \frac{D_{s12} \sin \alpha}{R_s} \frac{\partial \boldsymbol{\Phi}^T}{\partial x} \frac{\partial^2 \boldsymbol{\Phi}}{\partial x^2} \end{array} \right) R_s$$
$$+ \left(\begin{array}{l} D_{c11} \frac{\partial^2 \boldsymbol{\Phi}^T}{\partial x^2} \frac{\partial^2 \boldsymbol{\Phi}}{\partial x^2} + \frac{D_{c22} \sin^2 \alpha}{R_c^2} \frac{\partial \boldsymbol{\Phi}^T}{\partial x} \frac{\partial \boldsymbol{\Phi}}{\partial x} + \frac{A_{c22} \cos^2 \alpha}{R_c^2} \boldsymbol{\Phi}^T \boldsymbol{\Phi} \\ + \frac{D_{c12} \sin \alpha}{R_c} \frac{\partial^2 \boldsymbol{\Phi}^T}{\partial x^2} \frac{\partial \boldsymbol{\Phi}}{\partial x} + \frac{D_{c12} \sin \alpha}{R_c} \frac{\partial \boldsymbol{\Phi}^T}{\partial x} \frac{\partial^2 \boldsymbol{\Phi}}{\partial x^2} \end{array} \right) R_c$$
$$+ D_v c_x^2 \frac{\partial \boldsymbol{\Phi}^T}{\partial x} \frac{\partial \boldsymbol{\Phi}}{\partial x} R_v$$

$$-n > 0$$

$$\boldsymbol{K}_{bl} = \mathrm{diag} \, \pi \Big[k_{u0} \boldsymbol{\Phi}^T \boldsymbol{\Phi} R_{s0} \quad k_{v0} \boldsymbol{\Phi}^T \boldsymbol{\Phi} R_{s0} \quad k_{u0} \boldsymbol{\Phi}^T \boldsymbol{\Phi} R_{c0} \quad k_{v0} \boldsymbol{\Phi}^T \boldsymbol{\Phi} R_{c0}$$
$$k_{w0} \boldsymbol{\Phi}^T \boldsymbol{\Phi} (R_{s0} + R_{c0}) + K_{w0} \frac{\partial \boldsymbol{\Phi}^T}{\partial x} \frac{\partial \boldsymbol{\Phi}}{\partial x} (R_{s0} + R_{c0})$$
$$k_{u0} \boldsymbol{\Phi}^T \boldsymbol{\Phi} R_{s0} \quad k_{v0} \boldsymbol{\Phi}^T \boldsymbol{\Phi} R_{s0} \quad k_{u0} \boldsymbol{\Phi}^T \boldsymbol{\Phi} R_{c0} \quad k_{v0} \boldsymbol{\Phi}^T \boldsymbol{\Phi} R_{c0}$$
$$k_{w0} \boldsymbol{\Phi}^T \boldsymbol{\Phi} (R_{s0} + R_{c0}) + K_{w0} \frac{\partial \boldsymbol{\Phi}^T}{\partial x} \frac{\partial \boldsymbol{\Phi}}{\partial x} (R_{s0} + R_{c0}) \Big]_{x=0}$$

$$\boldsymbol{K}_{br} = \mathrm{diag} \, \pi \Big[k_{u1} \boldsymbol{\Phi}^T \boldsymbol{\Phi} R_{s1} \quad k_{v1} \boldsymbol{\Phi}^T \boldsymbol{\Phi} R_{s1} \quad k_{u1} \boldsymbol{\Phi}^T \boldsymbol{\Phi} R_{c1} \quad k_{v1} \boldsymbol{\Phi}^T \boldsymbol{\Phi} R_{c1}$$
$$k_{w1} \boldsymbol{\Phi}^T \boldsymbol{\Phi} (R_{s1} + R_{c1}) + K_{w1} \frac{\partial \boldsymbol{\Phi}^T}{\partial x} \frac{\partial \boldsymbol{\Phi}}{\partial x} (R_{s1} + R_{c1})$$
$$k_{u1} \boldsymbol{\Phi}^T \boldsymbol{\Phi} R_{s1} \quad k_{v1} \boldsymbol{\Phi}^T \boldsymbol{\Phi} R_{s1} \quad k_{u1} \boldsymbol{\Phi}^T \boldsymbol{\Phi} R_{c1} \quad k_{v1} \boldsymbol{\Phi}^T \boldsymbol{\Phi} R_{c1}$$
$$k_{w1} \boldsymbol{\Phi}^T \boldsymbol{\Phi} (R_{s1} + R_{c1}) + K_{w1} \frac{\partial \boldsymbol{\Phi}^T}{\partial x} \frac{\partial \boldsymbol{\Phi}}{\partial x} (R_{s1} + R_{c1}) \Big]_{x=L}$$

$$
\boldsymbol{K}_c = \pi \int_0^L
\begin{bmatrix}
k_{11} & k_{12} & k_{13} & k_{14} & \cdots & k_{110} \\
k_{12}^T & k_{22} & k_{23} & k_{24} & \cdots & k_{210} \\
k_{13}^T & k_{23}^T & k_{33} & k_{34} & \cdots & k_{310} \\
k_{14}^T & k_{24}^T & k_{34}^T & k_{44} & \cdots & k_{410} \\
\vdots & \vdots & \vdots & \vdots & \ddots & \vdots \\
k_{110}^T & k_{210}^T & k_{310}^T & k_{410}^T & \cdots & k_{1010}
\end{bmatrix} dx
$$

$$
k_{11} = k_{66} = \left(A_{s11} \frac{\partial \boldsymbol{\Phi}^T}{\partial x} \frac{\partial \boldsymbol{\Phi}}{\partial x} + \frac{A_{s66} n^2}{R_s^2} \boldsymbol{\Phi}^T \boldsymbol{\Phi} + \frac{A_{s22} \sin^2 \alpha}{R_s^2} \boldsymbol{\Phi}^T \boldsymbol{\Phi} + \frac{A_{s12} \sin \alpha}{R_s} \frac{\partial \boldsymbol{\Phi}^T}{\partial x} \boldsymbol{\Phi} \right. \\
\left. + \frac{A_{s12} \sin \alpha}{R_s} \boldsymbol{\Phi}^T \frac{\partial \boldsymbol{\Phi}}{\partial x} \right) R_s \\
+ \frac{D_v}{h_v^2} \boldsymbol{\Phi}^T \boldsymbol{\Phi} R_v
$$

$$
k_{12} = n \left(\frac{A_{s12}}{R_s} \frac{\partial \boldsymbol{\Phi}^T}{\partial x} \boldsymbol{\Phi} - \frac{A_{s66}}{R_s} \boldsymbol{\Phi}^T \frac{\partial \boldsymbol{\Phi}}{\partial x} + \frac{A_{s66} \sin \alpha}{R_s^2} \boldsymbol{\Phi}^T \boldsymbol{\Phi} + \frac{A_{s22} \sin \alpha}{R_s^2} \boldsymbol{\Phi}^T \boldsymbol{\Phi} \right) R_s
$$

$$
k_{13} = k_{68} - \frac{D_v}{h_v^2} \boldsymbol{\Phi}^T \boldsymbol{\Phi} R_v
$$

$$
k_{15} = k_{610} = \left(\frac{A_{s12} \cos \alpha}{R_s} \frac{\partial \boldsymbol{\Phi}^T}{\partial x} \boldsymbol{\Phi} + \frac{A_{s22} \sin \alpha \cos \alpha}{R_s^2} \boldsymbol{\Phi}^T \boldsymbol{\Phi} \right) R_s - \frac{D_v c_x}{h_v} \boldsymbol{\Phi}^T \frac{\partial \boldsymbol{\Phi}}{\partial x} R_v
$$

$$
k_{22} = k_{77} = \left(A_{s66} \frac{\partial \boldsymbol{\Phi}^T}{\partial x} \frac{\partial \boldsymbol{\Phi}}{\partial x} + \frac{A_{s22} n^2}{R_s^2} \boldsymbol{\Phi}^T \boldsymbol{\Phi} + \frac{A_{s66} \sin^2 \alpha}{R_s^2} \boldsymbol{\Phi}^T \boldsymbol{\Phi} - \frac{A_{s66} \sin \alpha}{R_s} \frac{\partial \boldsymbol{\Phi}^T}{\partial x} \boldsymbol{\Phi} \right. \\
\left. - \frac{A_{s66} \sin \alpha}{R_s} \boldsymbol{\Phi}^T \frac{\partial \boldsymbol{\Phi}}{\partial x} \right) R_s \\
+ D_v \left(\frac{1}{h_v} + \frac{\cos \alpha}{2R_v} \right)^2 \boldsymbol{\Phi}^T \boldsymbol{\Phi} R_v
$$

$$
k_{24} = k_{79} = -D_v \left(\frac{1}{h_v} - \frac{\cos \alpha}{2R_v} \right) \left(\frac{1}{h_v} + \frac{\cos \alpha}{2R_v} \right) \boldsymbol{\Phi}^T \boldsymbol{\Phi} R_v
$$

$$
k_{25} = \frac{n A_{s22} \cos \alpha}{R_s^2} \boldsymbol{\Phi}^T \boldsymbol{\Phi} R_s + n D_v c_\theta \left(\frac{1}{h_v} + \frac{\cos \alpha}{2R_v} \right) \boldsymbol{\Phi}^T \boldsymbol{\Phi} R_v
$$

$$
k_{33} = k_{88} = \left(A_{c11} \frac{\partial \boldsymbol{\Phi}^T}{\partial x} \frac{\partial \boldsymbol{\Phi}}{\partial x} + \frac{A_{c66} n^2}{R_c^2} \boldsymbol{\Phi}^T \boldsymbol{\Phi} + \frac{A_{c22} \sin^2 \alpha}{R_c^2} \boldsymbol{\Phi}^T \boldsymbol{\Phi} + \frac{A_{c12} \sin \alpha}{R_c} \frac{\partial \boldsymbol{\Phi}^T}{\partial x} \boldsymbol{\Phi} \right. \\
\left. + \frac{A_{c12} \sin \alpha}{R_c} \boldsymbol{\Phi}^T \frac{\partial \boldsymbol{\Phi}}{\partial x} \right) R_c \\
+ \frac{D_v}{h_v^2} \boldsymbol{\Phi}^T \boldsymbol{\Phi} R_v
$$

$$
k_{34} = n \left(\frac{A_{c12}}{R_c} \frac{\partial \boldsymbol{\Phi}^T}{\partial x} \boldsymbol{\Phi} - \frac{A_{c66}}{R_c} \boldsymbol{\Phi}^T \frac{\partial \boldsymbol{\Phi}}{\partial x} + \frac{A_{c66} \sin \alpha}{R_c^2} \boldsymbol{\Phi}^T \boldsymbol{\Phi} + \frac{A_{c22} \sin \alpha}{R_c^2} \boldsymbol{\Phi}^T \boldsymbol{\Phi} \right) R_c
$$

$$
k_{35} = k_{810} = \left(\frac{A_{c12} \cos \alpha}{R_c} \frac{\partial \boldsymbol{\Phi}^T}{\partial x} \boldsymbol{\Phi} + \frac{A_{c22} \sin \alpha \cos \alpha}{R_c^2} \boldsymbol{\Phi}^T \boldsymbol{\Phi} \right) R_c + \frac{D_v c_x}{h_v} \boldsymbol{\Phi}^T \frac{\partial \boldsymbol{\Phi}}{\partial x} R_v
$$

$$
k_{44} = k_{99} = \left(A_{c66} \frac{\partial \boldsymbol{\Phi}^T}{\partial x} \frac{\partial \boldsymbol{\Phi}}{\partial x} + \frac{A_{c22} n^2}{R_c^2} \boldsymbol{\Phi}^T \boldsymbol{\Phi} + \frac{A_{c66} \sin^2 \alpha}{R_c^2} \boldsymbol{\Phi}^T \boldsymbol{\Phi} - \frac{A_{c66} \sin \alpha}{R_c} \frac{\partial \boldsymbol{\Phi}^T}{\partial x} \boldsymbol{\Phi} \right. \\
\left. - \frac{A_{c66} \sin \alpha}{R_c} \boldsymbol{\Phi}^T \frac{\partial \boldsymbol{\Phi}}{\partial x} \right) R_c \\
+ D_v \left(\frac{1}{h_v} - \frac{\cos \alpha}{2R_v} \right)^2 \boldsymbol{\Phi}^T \boldsymbol{\Phi} R_v
$$

$$
k_{45} = \frac{n A_{c22} \cos \alpha}{R_c^2} \boldsymbol{\Phi}^T \boldsymbol{\Phi} R_c - n D_v c_\theta \left(\frac{1}{h_v} - \frac{\cos \alpha}{2R_v} \right) \boldsymbol{\Phi}^T \boldsymbol{\Phi} R_v
$$

$$
\begin{aligned}
k_{55} = k_{1010} = &\begin{pmatrix}
D_{s11}\dfrac{\partial^2 \mathbf{\Phi}^T}{\partial x^2}\dfrac{\partial^2 \mathbf{\Phi}}{\partial x^2} + \dfrac{D_{s22}n^4}{R_s^4}\mathbf{\Phi}\mathbf{\Phi} + \dfrac{D_{s22}\sin^2\alpha}{R_s^2}\dfrac{\partial \mathbf{\Phi}^T}{\partial x}\dfrac{\partial \mathbf{\Phi}}{\partial x} + \dfrac{4D_{s66}n^2\sin^2\alpha}{R_s^4}\mathbf{\Phi}^T\mathbf{\Phi} \\[2mm]
+\dfrac{A_{s22}\cos^2\alpha}{R_s^2}\mathbf{\Phi}^T\mathbf{\Phi} + \dfrac{4D_{s66}n^2}{R_s^2}\dfrac{\partial \mathbf{\Phi}^T}{\partial x}\dfrac{\partial \mathbf{\Phi}}{\partial x} + \dfrac{D_{s12}\sin\alpha}{R_s}\dfrac{\partial^2 \mathbf{\Phi}^T}{\partial x^2}\dfrac{\partial \mathbf{\Phi}}{\partial x} \\[2mm]
+\dfrac{D_{s12}\sin\alpha}{R_s}\dfrac{\partial \mathbf{\Phi}^T}{\partial x}\dfrac{\partial^2 \mathbf{\Phi}}{\partial x^2} - \dfrac{D_{s12}n^2}{R_s^2}\dfrac{\partial^2 \mathbf{\Phi}^T}{\partial x^2}\mathbf{\Phi} - \dfrac{D_{s12}n^2}{R_s^2}\mathbf{\Phi}^T\dfrac{\partial^2 \mathbf{\Phi}}{\partial x^2} - \dfrac{D_{s22}n^2\sin\alpha}{R_s^3}\dfrac{\partial \mathbf{\Phi}^T}{\partial x}\mathbf{\Phi} \\[2mm]
-\dfrac{D_{s11}n^2\sin\alpha}{R_s^3}\mathbf{\Phi}^T\dfrac{\partial \mathbf{\Phi}}{\partial x} - \dfrac{4D_{s66}n^2\sin\alpha}{R_s^3}\mathbf{\Phi}^T\dfrac{\partial \mathbf{\Phi}}{\partial x} - \dfrac{4D_{s66}n^2\sin\alpha}{R_s^3}\dfrac{\partial \mathbf{\Phi}^T}{\partial x}\mathbf{\Phi}
\end{pmatrix}R_s \\[4mm]
+ &\begin{pmatrix}
D_{c11}\dfrac{\partial^2 \mathbf{\Phi}^T}{\partial x^2}\dfrac{\partial^2 \mathbf{\Phi}}{\partial x^2} + \dfrac{D_{c22}n^4}{R_c^4}\mathbf{\Phi}\mathbf{\Phi} + \dfrac{D_{c22}\sin^2\alpha}{R_c^2}\dfrac{\partial \mathbf{\Phi}^T}{\partial x}\dfrac{\partial \mathbf{\Phi}}{\partial x} + \dfrac{4D_{c66}n^2\sin^2\alpha}{R_c^4}\mathbf{\Phi}^T\mathbf{\Phi} \\[2mm]
+\dfrac{A_{c22}\cos^2\alpha}{R_c^2}\mathbf{\Phi}^T\mathbf{\Phi} + \dfrac{4D_{c66}n^2}{R_c^2}\dfrac{\partial \mathbf{\Phi}^T}{\partial x}\dfrac{\partial \mathbf{\Phi}}{\partial x} + \dfrac{D_{c12}\sin\alpha}{R_c}\dfrac{\partial^2 \mathbf{\Phi}^T}{\partial x^2}\dfrac{\partial \mathbf{\Phi}}{\partial x} + \dfrac{D_{c12}\sin\alpha}{R_c}\dfrac{\partial \mathbf{\Phi}^T}{\partial x}\dfrac{\partial^2 \mathbf{\Phi}}{\partial x^2} \\[2mm]
-\dfrac{D_{c12}n^2}{R_c^2}\dfrac{\partial^2 \mathbf{\Phi}^T}{\partial x^2}\mathbf{\Phi} - \dfrac{D_{c12}n^2}{R_c^2}\mathbf{\Phi}^T\dfrac{\partial^2 \mathbf{\Phi}}{\partial x^2} - \dfrac{D_{c22}n^2\sin\alpha}{R_c^3}\dfrac{\partial \mathbf{\Phi}^T}{\partial x}\mathbf{\Phi} - \dfrac{D_{c11}n^2\sin\alpha}{R_c^3}\mathbf{\Phi}^T\dfrac{\partial \mathbf{\Phi}}{\partial x} \\[2mm]
-\dfrac{4D_{c66}n^2\sin\alpha}{R_c^3}\mathbf{\Phi}^T\dfrac{\partial \mathbf{\Phi}}{\partial x} - \dfrac{4D_{c66}n^2\sin\alpha}{R_c^3}\dfrac{\partial \mathbf{\Phi}^T}{\partial x}\mathbf{\Phi}
\end{pmatrix}R_c \\[4mm]
+ &\left(D_v c_x^2 \dfrac{\partial \mathbf{\Phi}^T}{\partial x}\dfrac{\partial \mathbf{\Phi}}{\partial x} + D_v c_\theta^2 n^2 \mathbf{\Phi}^T\mathbf{\Phi} \right) R_v
\end{aligned}
$$

$$
k_{67} = n\left(-\dfrac{A_{s12}}{R_s}\dfrac{\partial \mathbf{\Phi}^T}{\partial x}\mathbf{\Phi} + \dfrac{A_{s66}}{R_s}\mathbf{\Phi}^T\dfrac{\partial \mathbf{\Phi}}{\partial x} - \dfrac{A_{s66}\sin\alpha}{R_s^2}\mathbf{\Phi}^T\mathbf{\Phi} - \dfrac{A_{s22}\sin\alpha}{R_s^2}\mathbf{\Phi}^T\mathbf{\Phi} \right) R_s
$$

$$
k_{710} = -\dfrac{nA_{s22}\cos\alpha}{R_s^2}\mathbf{\Phi}^T\mathbf{\Phi}R_s - nD_v c_\theta \left(\dfrac{1}{h_v} + \dfrac{\cos\alpha}{2R_v} \right)\mathbf{\Phi}^T\mathbf{\Phi}R_v
$$

$$
k_{89} = n\left(-\dfrac{A_{c12}}{R_c}\dfrac{\partial \mathbf{\Phi}^T}{\partial x}\mathbf{\Phi} + \dfrac{A_{c66}}{R_c}\mathbf{\Phi}^T\dfrac{\partial \mathbf{\Phi}}{\partial x} - \dfrac{A_{c66}\sin\alpha}{R_c^2}\mathbf{\Phi}^T\mathbf{\Phi} - \dfrac{A_{c22}\sin\alpha}{R_c^2}\mathbf{\Phi}^T\mathbf{\Phi} \right) R_c
$$

$$
k_{910} = -\dfrac{nA_{c22}\cos\alpha}{R_c^2}\mathbf{\Phi}^T\mathbf{\Phi}R_c + nD_v c_\theta \left(\dfrac{1}{h_v} - \dfrac{\cos\alpha}{2R_v} \right)\mathbf{\Phi}^T\mathbf{\Phi}R_v
$$

Other elements of the matrix $\mathbf{K}$ are zero.

Appendix 2. The components of the mass matrix M

$-n = 0$

$$
\mathbf{M} = \int_0^L \mathbf{\Phi}^T\mathbf{\Phi}\{\mathrm{diag}[\rho_s h_s R_s \quad \rho_s h_s R_s \quad \rho_c h_c R_c \quad \rho_c h_c R_c \quad \rho_s h_s R_s + \rho_v h_v R_v + \rho_c h_c R_c]\}\mathrm{d}x
$$

$-n > 0$

$$
\mathbf{M} = \pi \int_0^L \mathbf{\Phi}^T\mathbf{\Phi}\left\{ \mathrm{diag}\begin{bmatrix} \rho_s h_s R_s & \rho_s h_s R_s & \rho_c h_c R_c & \rho_c h_c R_c & \rho_s h_s R_s + \rho_v h_v R_v + \rho_c h_c R_c \\ \rho_s h_s R_s & \rho_s h_s R_s & \rho_c h_c R_c & \rho_c h_c R_c & \rho_s h_s R_s + \rho_v h_v R_v + \rho_c h_c R_c \end{bmatrix} \right\}\mathrm{d}x
$$

References

1. A. Yadav, M. Amabili, S.K. Panda, Forced nonlinear vibrations of circular cylindrical sandwich shells with cellular core using higher-order shear and thickness deformation theory. Compos. Struct. **510**, 116283 (2021)
2. C. Yang, G. Jin, Y. Zhang, Z. Liu, A unified three-dimensional method for vibration analysis of the frequency-dependent sandwich shallow shells with general boundary conditions. Appl. Math. Model. **66**, 59–76 (2019)
3. Y.S. Li, B.L. Liu, Thermal buckling and free vibration of viscoelastic functionally graded sandwich shells with tunable auxetic honeycomb core. Appl. Math. Model. **108**, 685–700 (2022)
4. G. Wang, H. Li, Y. Yang, Z. Qiao, Nonlinear vibration characteristics of composite pyramidal truss sandwich cylindrical shell panels with amplitude dependence. Appl. Math. Model. (2023). https://doi.org/10.1016/j.apm.2023.02.020

5. Q. Wang, X. Cui, B. Qin, Q. Liang, J. Tang, A semi-analytical method for vibration analysis of functionally graded (FG) sandwich doubly-curved panels and shells of revolution. Int. J. Mech. Sci. **134**, 479–499 (2017)
6. C. Yang, G. Jin, Z. Liu, X. Wang, X. Miao, Vibration and damping analysis of thick sandwich cylindrical shells with a viscoelastic core under arbitrary boundary conditions. Int. J. Mech. Sci. **92**, 162–177 (2015)
7. E. Taati, F. Fallah, M.T. Ahmadian, Subsonic and supersonic flow-induced vibration of sandwich cylindrical shells with FG-CNT reinforced composite face sheets and metal foam core. Int. J. Mech. Sci. **215**, 106918 (2022)
8. E. Taati, F. Fallah, M.T. Ahmadian, On nonlinear free vibration of externally compressible fluid-loaded sandwich cylindrical shells: curvature nonlinearity in bending and impermeability condition. Thin Walled Struct. **179**, 109599 (2022)
9. J. Yang, J. Xiong, Li. Ma, G. Zhang, X. Wang, Wu. Linzhi, Study on vibration damping of composite sandwich cylindrical shell with pyramidal truss-like cores. Compos. Struct. **117**, 362–372 (2014)
10. M. Karimiasl, F. Ebrahimi, Large amplitude vibration of viscoelastically damped multiscale composite doubly curved sandwich shell with flexible core and MR layers. Compos. Struct. **117**, 362–372 (2014)
11. Y. Li, W. Yao, T. Wang, Large amplitude vibration of Free flexural vibration of thin-walled honeycomb sandwich cylindrical shells. Thin Walled Struct. **157**, 107032 (2022)
12. T. Fu, X. Wu, Z. Xiao, Z. Chen, B. Li, Analysis of vibration characteristics of FGM sandwich joined conical-conical shells surrounded by elastic foundations. Thin Walled Struct. **165**, 107979 (2021)
13. E. Sobhani, Vibrational characteristics of fastening of a spherical shell with a coupled conical-conical shells strengthened with nanocomposite sandwiches contained agglomerated CNT face layers and GNP core under spring boundary conditions. Eng. Anal. Bound. Elem. **146**, 362–387 (2023)
14. A. Kumar, A. Chakrabarti, P. Bhargava, Vibration of laminated composites and sandwich shells based on higher order zigzag theory. Thin Walled Struct. **56**, 880–888 (2013)
15. T.D. Singhaa, M. Rout, Free vibration analysis of rotating pretwisted composite sandwich conical shells with multiple debonding in hygrothermal environment. Eng. Struct. **204**, 110058 (2020)
16. H. Li, B. Dong, J. Zhao, Z. Zou, Nonlinear free vibration of functionally graded fiber-reinforced composite hexagon honeycomb sandwich cylindrical shells. Eng. Struct. **263**, 114372 (2022)
17. H.-A. Pham, H.-Q. Tran, M.-T. Tran, V.-L. Nguyen, Free vibration analysis and optimization of doubly-curved stiffened sandwich shells with functionally graded skins and auxetic honeycomb core layer. Eng. Struct. **263**, 114372 (2022)
18. E. Sobhani, A.R. Masoodi, A.R. Ahmadi-Pari, Circumferential vibration analysis of nano-porous-sandwich assembled spherical-cylindrical-conical shells under elastic boundary conditions. Eng. Struct. **273**, 115094 (2022)
19. E. Sobhani, A.R. Masoodi, A.R. Ahmadi-Pari, Vibration of FG-CNT and FG-GNP sandwich composite coupled conical–cylindrical–conical shell. Eng. Struct. **273**, 114281 (2021)
20. X. Xue, C. Zheng, F.-Q. Lai, Wu. Xue-qian, Mechanical property of cylindrical sandwich shell with gradient core of entangled wire mesh. Def. Technol. (2023). https://doi.org/10.1016/j.dt.2023.01.003
21. A.H. Sofiyev, The vibration and buckling of sandwich cylindrical shells covered by different coatings subjected to the hydrostatic pressure. Compos. Struct. **117**, 124–134 (2014)
22. H. Chen, A. Wanga, Y. Hao, W. Zhang, Free vibration of FGM sandwich doubly-curved shallow shell based on a new shear deformation theory with stretching effects. Compos. Struct. **179**, 50–60 (2017)
23. Bo. Liu, M. Guo, C. Liu, Y. Xing, Free vibration of functionally graded sandwich shallow shells in thermal environments by a differential quadrature hierarchical finite element method. Compos. Struct. **225**, 111173 (2019)
24. M. Karimiasla, F. Ebrahimia, V. Mahesh, Nonlinear forced vibration of smart multiscale sandwich composite doubly curved porous shell. Thin Walled Struct. **143**, 106512 (2019)
25. Qi. He, Y.-L. Zhou, M. Li, L. He, H.-L. Dai, Nonlinear vibration analysis of CFRR sandwich doubly-curved shallow shells with a porous microcapsule coating in hygrothermal environment. Thin Walled Struct. **185**, 110587 (2023)
26. A.S. Sayyad, Y.M. Ghugal, Static and free vibration analysis of laminated composite and sandwich spherical shells using a generalized higher-order shell theory. Compos. Struct. **219**, 129–146 (2019)
27. M. Chehreghani, M.D. Pazhooh, M. Shakeri, Vibration analysis of a fluid conveying sandwich cylindrical shell with a soft Core. Compos. Struct. **230**, 111470 (2019)
28. T.D. Singha, M. Rout, T. Bandyopadhyay, A. Karmakar, Free vibration of rotating pretwisted FG-GRC sandwich conical shells inthermal environment using HSDT. Compos. Struct. **257**, 113144 (2021)
29. F. Bahranifard, P. Malekzadeh, M.R. Golbahar Haghighi, Moving load response of ring-stiffened sandwich truncated conical shells with GPLRC face sheets and porous core. Thin Walled Struct. **180**, 109984 (2022)
30. D.G. Ninh, N.H. Ha, N.T. Long, Thermal vibrations of complex-generatrix shells made of sandwich CNTRC sheets on both sides and open/closed cellular functionally graded porous core. Thin Walled Struct. **182**, 110161 (2023)
31. A.H. Sofiyev, E. Osmancelebioglu, The free vibration of sandwich truncated conical shells containing functionally graded layers within the shear deformation theory. Compos. Part B **120**, 197–211 (2017)
32. H. Li, D. Liu, B. Dong, K. Sun, Investigation of vibration suppression performance of composite pyramidal truss sandwich cylindrical shell panels with damping coating. Thin Walled Struct. **181**, 109980 (2022)
33. W. Zheng, J. Liu, M.A. Oyarhossein, Prediction of nth-order derivatives for vibration responses of a sandwich shell composed of a magnetorheological core and composite face layers. Eng. Anal. Bound. Elem. **146**, 170–183 (2023)
34. D.K. Biswal, S. Chandra, Free vibration and damping characteristics study of doubly curved sandwich shell panels with viscoelastic core and isotropic/laminated constraining layer. Eur. J. Mech. A. Solids **72**, 424–439 (2018)
35. R. Suresh Kumar, S.I. Kundalwal, M.C. Ray, Control of large amplitude vibrations of doubly curved sandwich shells composed of fuzzy fiber reinforced composite facings. Aerosp. Sci. Technol. **70**, 10–28 (2017)
36. A.H. Soureshjani, R. Talebitooti, M. Talebitooti, A semi-analytical approach on the effect of external lateral pressure on free vibration of joined sandwich aerospace composite conical-conical shells. Aerosp. Sci. Technol. **70**, 10–28 (2017)
37. A. Aliyari Parand, A. Alibeigloo, Static and vibration analysis of sandwich cylindrical shell with functionally graded core and viscoelastic interface using DQM. Compos. Part B **126**, 1–16 (2017)
38. A.R. Setoodeh, M. Shojaee, P. Malekzadeh, Vibrational behavior of doubly curved smart sandwich shells with FGCNTRC face sheets and FG porous core. Compos. Part B **165**, 798–822 (2019)
39. N.K. Sahu, D.K. Biswal, S.V. Joseph, S.C. Mohanty, Vibration and damping analysis of doubly curved viscoelastic-FGM sandwich shell structures using FOSDT. Structures **26**, 24–38 (2020)

40. G. Jin, C. Yang, Z. Liu, S. Gao, C. Zhang, A unified method for the vibration and damping analysis of constrained layer damping cylindrical shells with arbitrary boundary conditions. Compos. Struct. **130**, 124–142 (2015)